Another Wintertime Cloud Seeding Case Study with Strong Evidence of Seeding Effects

Arlen W. Huggins
Desert Research Institute
Reno, NV

Abstract. In the 1990s numerous winter orographic cloud seeding experiments were conducted over Utah's Wasatch Plateau. Several previously published case studies successfully documented the physical response in clouds and precipitation to ground-based seeding with silver iodide and liquid propane. A previously unpublished case study that shows additional evidence of positive seeding effects is presented here. Careful documentation of seeding plume transport and dispersion coupled with aircraft and ground-based measurements within and outside the seeding plume are used to verify the steps in the conceptual model for orographic cloud seeding. It is shown that seeding produced significant increases in ice crystal concentrations (well above 10 times the natural background at aircraft level) and strong indications of increased precipitation at the surface (> 3 times the precipitation rate measured outside the seeding plume). Compared to other Utah results, the most unique aspect of this case study was the apparent detection of the seeding effect in the data from the project K_a-band radar. The radar seeding signature documented the areal extent and duration of the seeding effect in a way that was not previously possible using the more intermittent aircraft measurements and the lower spatial resolution precipitation data. The physical evidence of seeding effects documented in this and several other Utah/NOAA experiments supports the development of a larger scale randomized experiment to satisfy the call for proof of cloud seeding effectiveness in a recent National Academies of Science report.

1. Introduction and Background

The recent National Academies of Science (NAS) report (NRC, 2003) on critical issues in weather modification research concluded that there "is no convincing scientific proof of the efficacy of intentional weather modification efforts." The report further stated that, "In some instances there are strong indications of induced changes, but this evidence has not been subjected to tests of significance and reproducibility." This paper deals with seeding of winter orographic cloud systems, which the NAS report actually admitted showed "strong suggestions of positive seeding effects". In fact there were numerous carefully conducted winter orographic cloud seeding experiments in the 1980s, 1990s, and early 2000s, and these experiments contributed much of the positive evidence referred to in the NAS report. In many instances the results of small scale experiments were repeatable, and in some randomized experiments the results were also statistically significant.

If careful attention is paid to the work done during the Bridger Range Experiment (BRE) in Montana (Super, 1974; Super and Heimbach, 1983; and Super and Heimbach, 1988), there is to be found not only strong evidence of seeding effects but repeatable documentation of most of the "links-in-the-chain" of the cloud seeding processes, from the transport and dispersion of seeding material to the target, to the development of ice crystals in seeded cloud zones, to the fallout of ice crystals over the target. Seeding experiments over the Grand Mesa of Colorado (Holroyd et al., 1988 and Super and Boe, 1988) produced similar results and carried the "links-in-the-chain" to the surface where detectable increases in precipitation were noted. In the 1990s winter seeding experiments were conducted within the National Oceanic and Atmospheric Administration's (NOAA) Atmospheric Modification Program (AMP). Using an experimental design similar to that used in the BRE, ground seeding experiments were carried out over the Wasatch Plateau as part of the Utah/NOAA AMP. Here mobile ground-based instrument platforms, instrumented aircraft and remote sensing instruments provided possibly the best physical evidence to date of seeding effects in winter orographic cloud systems. The Utah work is summarized by Super (1999).

Although the bulk of the evidence of cloud seeding effects from the Utah AMP came from ground and aircraft laser imaging probes and precipitation gages, one case, only previously examined in a conference proceedings (Huggins, 1996), also showed seeding effects in the data from a K_a-band radar (wavelength 8.6 mm) operated in the project area. Because the signal backscattered to a radar is most strongly influenced by particle size

(a diameter to the sixth power dependency), seeding effects which are typically initially characterized by an abundance of small ice crystals (Super, 1999) tend to produce weak radar returns that can easily be obscured by the return from natural snowfall containing much larger ice crystals. The cloud seeding case to be described took place during a period of relatively shallow orographic cloud and very light and sporadic natural precipitation, a situation recognized previously (*e.g.*, Rauber et al., 1986) as having very good seeding potential.

This paper describes effects from silver iodide (AgI) ground seeding that include documentation of the transport and dispersion of the seeding material, ice crystal enhancement observed by aircraft particle probes, and precipitation enhancement detectable in the surface gage network. The seeding effect noted by the K_a-band radar adds another aspect to the observations by showing the areal coverage of the seeding effect, and the best evidence to date of the size and shape of the fallout region of ice crystals from a seeding plume.

2. Description of Project Area and Instrumentation

The Wasatch Plateau project area has been described in many other papers (*e.g.*, Holroyd et al., 1995). Briefly, a mobile radiometer was based at HQ in Fig. 1 and was driven on Highways 31 and 264 on the Wasatch Plateau to document the spatial distribution of supercooled cloud water (Huggins, 1995). A van instrumented with a sulfur hexaflouride (SF_6) detector, an NCAR ice nucleus counter, a Particle Measurement System (PMS) 2D-C probe, and standard meteorological instruments was also based at HQ and driven over the same routes during storms and cloud seeding experiments. A NOAA research aircraft was used for airborne plume tracking and cloud microphysics studies, and flew the tracks shown in Fig. 1 plus a cross-barrier track and a third barrier-parallel track between the west and east tracks. Figure 2 shows a vertical cross-section of the plateau with instrumentation sites and aircraft tracks. The aircraft recorded standard meteorological data as well as liquid water content (King probe), ice crystal imagery (PMS 2D-C), SF_6 concentration (Scientech LBF-3 detector), horizontal winds, and position (LORAN and GPS). An FAA waiver allowed the NOAA aircraft to fly within 1000 feet of the highest terrain on the plateau, thereby providing a much better chance of sampling the cloud layer where the bulk of the supercooled liquid water (SLW) and seeding material has been shown to exist (*e.g.*, Heggli and Rauber, 1988 and Huggins, 1995).

The radar-radiometer site (RRS in Fig. 1) was equipped with standard meteorological instruments, a fixed-position microwave radiometer (operated with zenith-pointing antenna), scanning K_a-band radar, and an NCAR ice nucleus counter. The scanning radar was added to the program in 1994 for the purpose of monitoring natural cloud conditions, tracking chaff plumes in clear weather conditions, and for the possible detection of ice crystals in seeding plumes during experiments conducted in lightly or non-precipitating clouds. The fixed target site (TAR in Fig. 1) also had a standard set of meteorological instruments, plus an NCAR counter and tower-mounted 2D-C probe. Precipitation microphysics observations were made at TAR, and sequential snow samples were collected for later trace chemical analysis for silver content. A Doppler acoustic sounder was operated on top of the plateau near the "X" northeast of RRS in Fig. 1. Precipitation gages on the plateau were standard weighing Belfort gages modified with 12-inch orifices to increase their resolution.

Two types of seeding generators were operated at HAS and AHS. One was a Desert Research Institute (DRI) remotely-controlled unit which burned a solution of AgI-NH_4I in acetone, which produces a contact type of ice nucleus (DeMott, 1983). This same mixture was used by the Utah operational project in the 1990s. The DRI generators were set to release AgI at a rate of 22.5 g h^{-1}. In addition both sites had Montana State University (MSU) manually operated generators that burned the same seeding solution and released AgI at 30 g h^{-1}. The Colorado State University Cloud Simulation and Aerosol Laboratory cloud chamber calibration for this seeding solution in the MSU generator indicated ice nucleus productions of about $3x10^{14}$, $6x10^{13}$, and $2x10^{12}$ nuclei per gram of AgI at activation temperatures of -12^{o}, -10^{o} and -8^{o} C, respectively (at natural wind tunnel drafts of 1-2 m s^{-1}).

The combination of ground-based mobile platforms, the radar, the aircraft and the stationary instrument sites has been shown to be very effective in documenting seeding plume positions and quantifying cloud and precipitation parameters inside and outside of seeding plumes (Super, 1999). The following sections describe the previously unpublished silver iodide seeding experiment conducted on 19 February 1994.

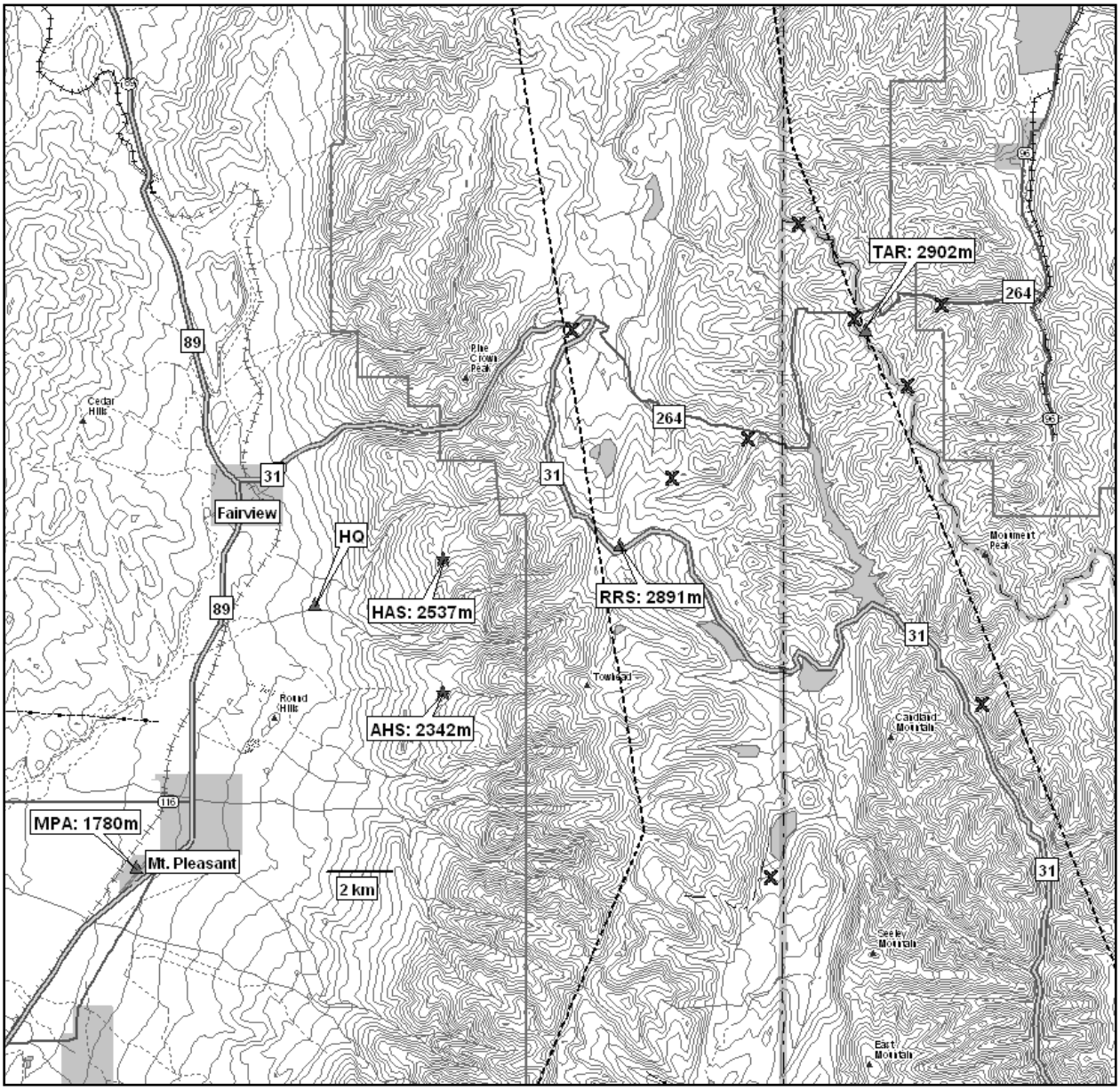

Figure 1. Map of the Utah Wasatch Plateau project area. Primary ground-based instruments were located at the radar-radiometer site (RRS) and the target site (TAR). Mobile data collections were along the highways labeled 31 and 264. The two high altitude seeding sites were at HAS and AHS. The upper air sounding site was at MPA. Precipitation gage sites are marked by an X. The west and east research aircraft flight tracks are shown by the dashed lines near the center and right side of the map. The map scale is indicated by the line segment labeled 2 km to the right of Mt. Pleasant. Height contour interval is 40m.

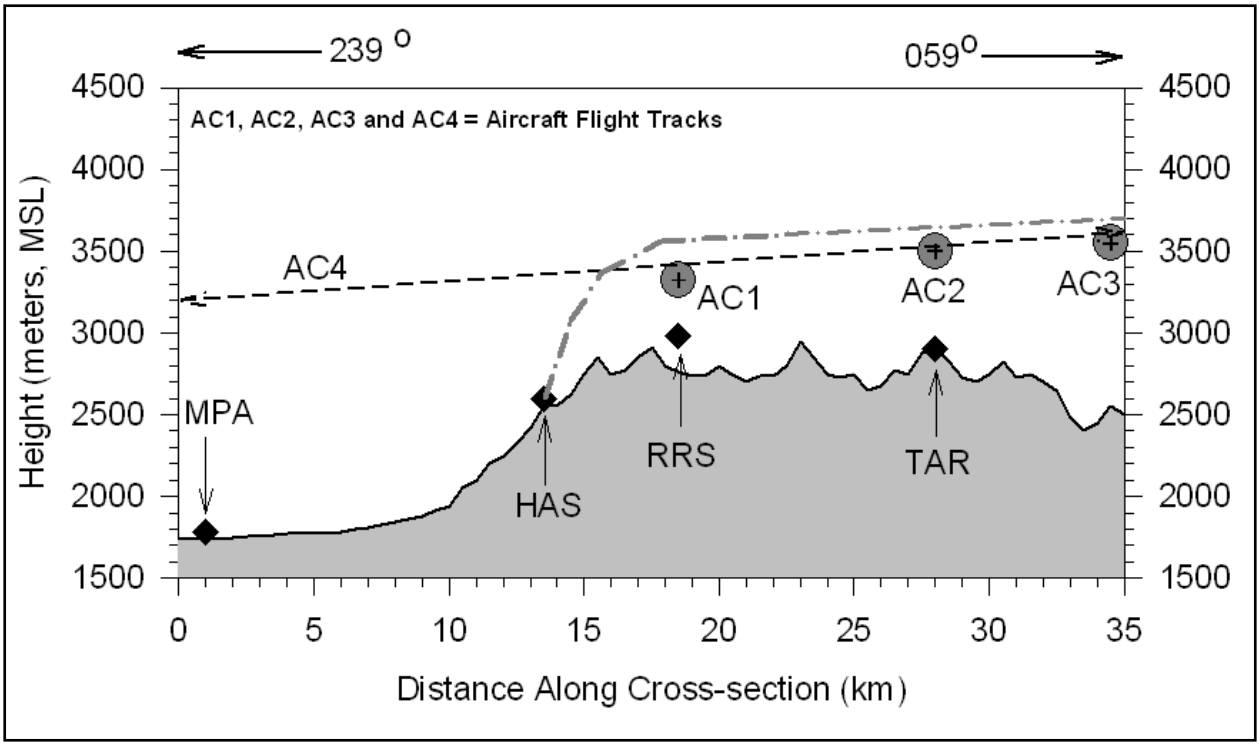

Figure 2. A southwest (left) to northeast (right) cross-section of the Wasatch Plateau constructed roughly along a line from the upper air sounding site (MPA) through the target site (TAR) as shown in Fig. 1. The horizontal positions of flight tracks AC1 and AC2 are also shown in Fig. 1. The dot-dash line emanating from HAS shows the approximate top of a typical silver iodide plume as determined from numerous Utah seeding experiments.

3. Meteorological Conditions and Seeding Operations on 19 February 1994

On 19 February 1994 the western U. S. was under the influence of a very broad and deep trough with the strongest height gradient and winds located well south of Utah over southern Arizona and New Mexico. The passage of a weak shortwave early on 19 February created more of a split flow pattern over the Great Basin, resulting in a relatively weak wind field and cold temperatures over western to central Utah. The weather pattern is shown by the satellite image and 700 mb map composite in Fig. 3. A large cloud mass with some cloud tops colder than -30°C had just moved past the RRS leaving behind clouds with tops generally warmer than -20° C, that included a few small cloud band features west of the project area. The bottom panel of Fig. 3 shows the cloud field at the start of the seeding experiment on 19 February.

An extensive but shallow layer of moisture covered most of the Great Basin, and the advection of this moisture over the Wasatch Plateau led to shallow orographic cloud development with some embedded convection as the upper trough gradually moved eastward during the day. A project sounding taken from MPA at 0900 (all times MST) is shown in Fig. 4. The sounding showed neutral stability in a moist layer from 2000 to 4000 m with winds from 235-255° at 5-6 m s^{-1} in the same layer. A sounding at 1100 (not shown) near the end of the seeding period showed convectively unstable conditions in a similar moist layer with winds from 220° at 5 m s^{-1} at 2200 m and from 245° at 6 m s^{-1} at the top of the moist layer at 3800 m. The moist layer was capped by much drier air and a slight inversion was apparent at 1100. Doppler sounder winds in the 300 m layer above the plateau top were 230-250° at 3-6 m s^{-1} between 0700 and 1000, then backed somewhat to 200-210° in the lowest 200m in the period from 1000 to 1200.

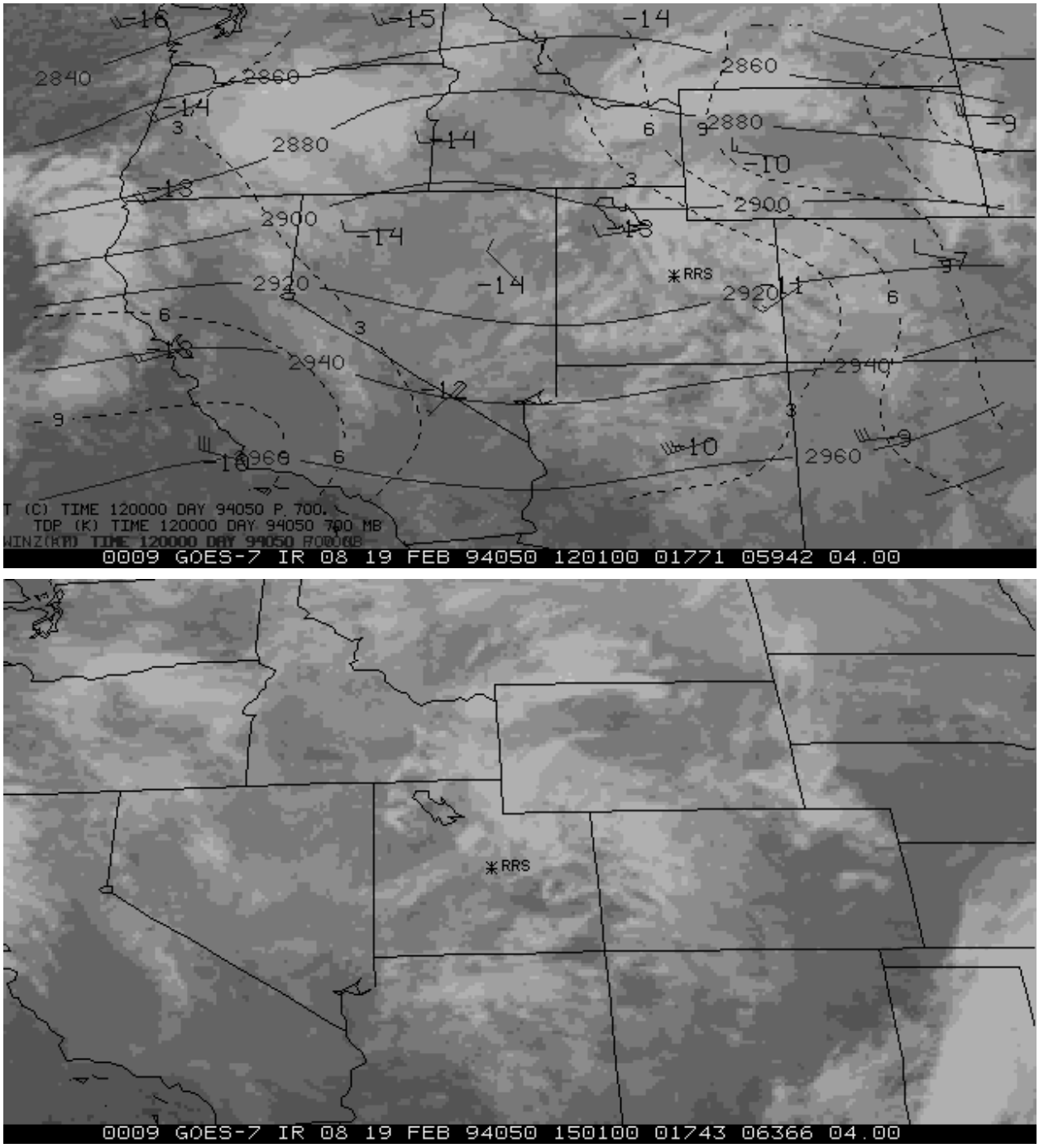

Figure 3. Top: Composite of an infrared satellite image and 700 mb plot for 1200 UTC on 19 February 1994. Dashed lines are dew point depression contours, black lines are geopotential height in meters. Wind barbs and temperatures are shown at NWS upper air sites. Bottom: Infrared satellite image taken at the beginning of the AgI seeding experiment at1500 UTC on 19 February. RRS site from Fig. 1 is shown in both images.

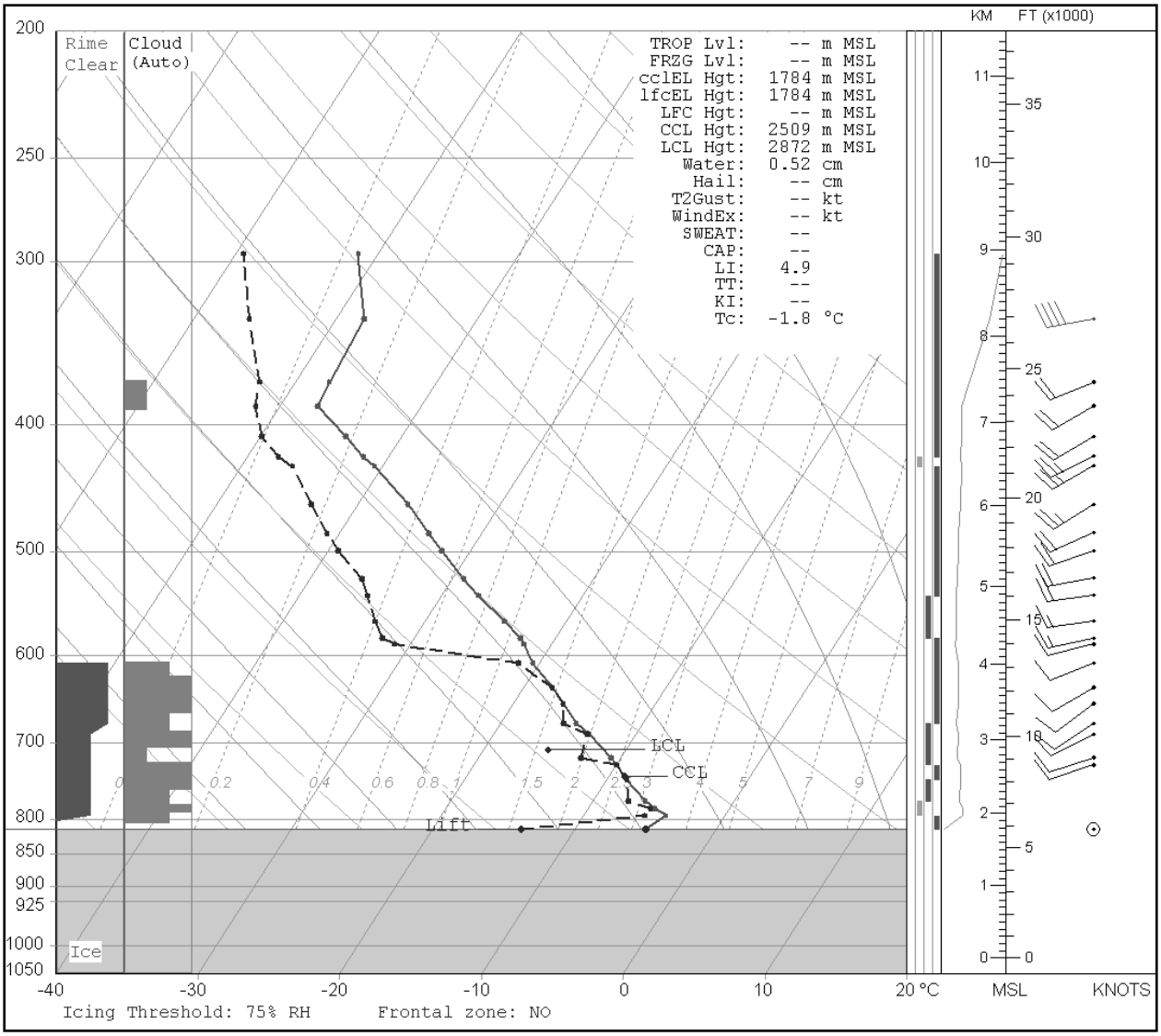

Figure 4. Skew-T Log-P thermodynamic diagram of an upper air sounding taken upwind of the Utah Wasatch Plateau (from site MPA in Fig. 1) on 19 February 1994 at 0900 MST. Analyses from the RAOB program (ERS, 2003) show the estimated depth of cloud and icing layers at the left side of the plot and the lifted condensation and convective condensation heights on the temperature profile.

Figures 5, 6 and 7 show the meteorological conditions at HAS, RRS and TAR from 0700 to 1200, the period surrounding the experimental seeding period. Winds at HAS were 2-3 m s^{-1} lighter than sounding winds at the same level, but were from about the same direction (averaging about 230°). RRS winds ranged from 245-260° at 5-6 m s^{-1}, quite similar to sounding winds at the level of the plateau top. The wind observed at TAR was more westerly (260-280°) and somewhat stronger (6-9 m s^{-1}) than the wind on the upwind side of the Plateau.

Supercooled liquid water depth measured by the RRS radiometer gradually decreased from 0.4 mm at 0700 to about 0.1 mm near the end of the seeding period at 1000. Sporadic instances of 0.2-0.4 mm were noted after 1000, suggesting clouds had become more convective with time. The temperature at the seeding site (HAS) increased steadily from -10° C at 0700 to -5° C at about 1100. The temperature at RRS (Fig. 6) rose very gradually from -12° C to about -11° C between 0700 and 1200, with the trend at TAR being

nearly identical but about 0.5° colder than RRS. The icing detector "trips" shown in Fig. 6 indicate that RRS was in cloud at least occasionally during the seeding period. Finally, the scientist onboard the NOAA aircraft noted cloud tops were generally near the highest track altitude (3750 m) at about -17° C. The aircraft King probe liquid water contents reached peaks of 0.3-0.5 g m^{-3} in the altitude layer from 3200 m to 3750 m.

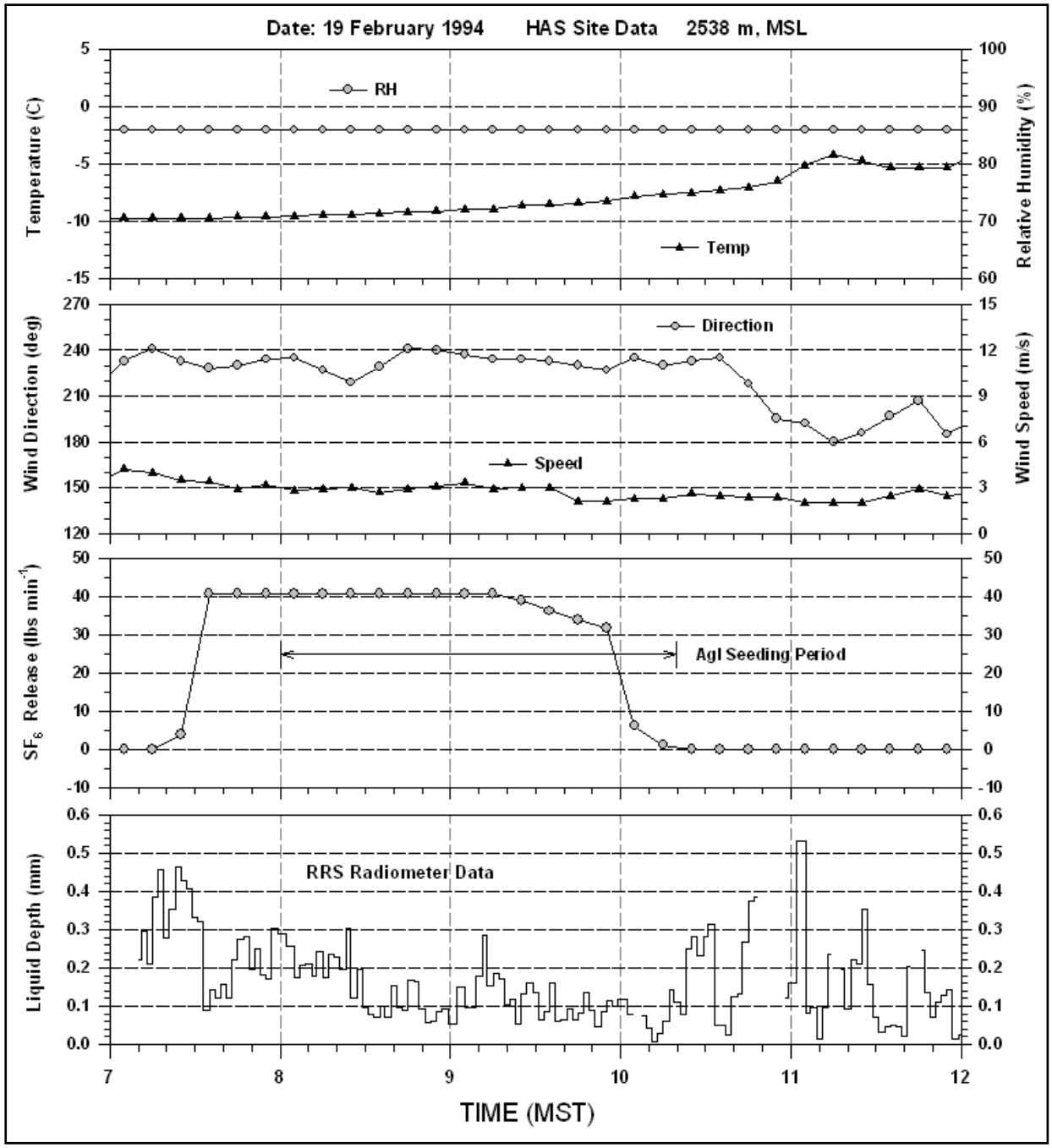

Figure 5. Meteorological and seeding operations data from the HAS site (top 3 panels) and radiometer data from RRS (bottom panel). Note that lack of change in relative humidity data suggests the sensor was at the upper limit of its operating range (*i.e.*, near water saturation).

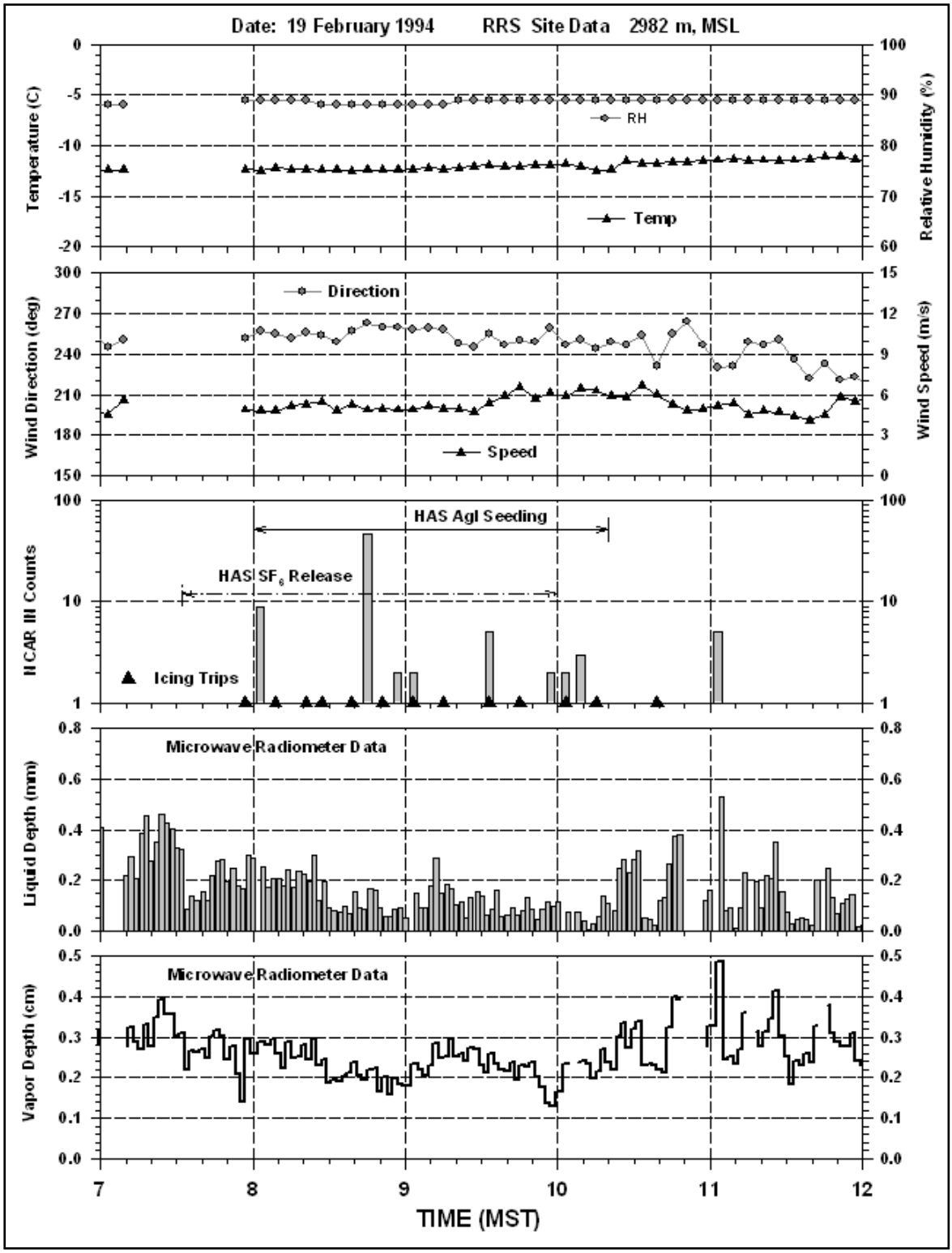

Figure 6. Meteorological data, ice nucleus counts, and radiometer data observed at RRS from 1400 to 1900 UTC on 19 February 1994. Third panel also shows SF_6 and AgI release periods from HAS. Note as with RH sensor at HAS that the reading of ~90% is likely at the upper range of the sensor since third panel shows icing occurred between 1500 and 1900 (indicating saturated conditions).

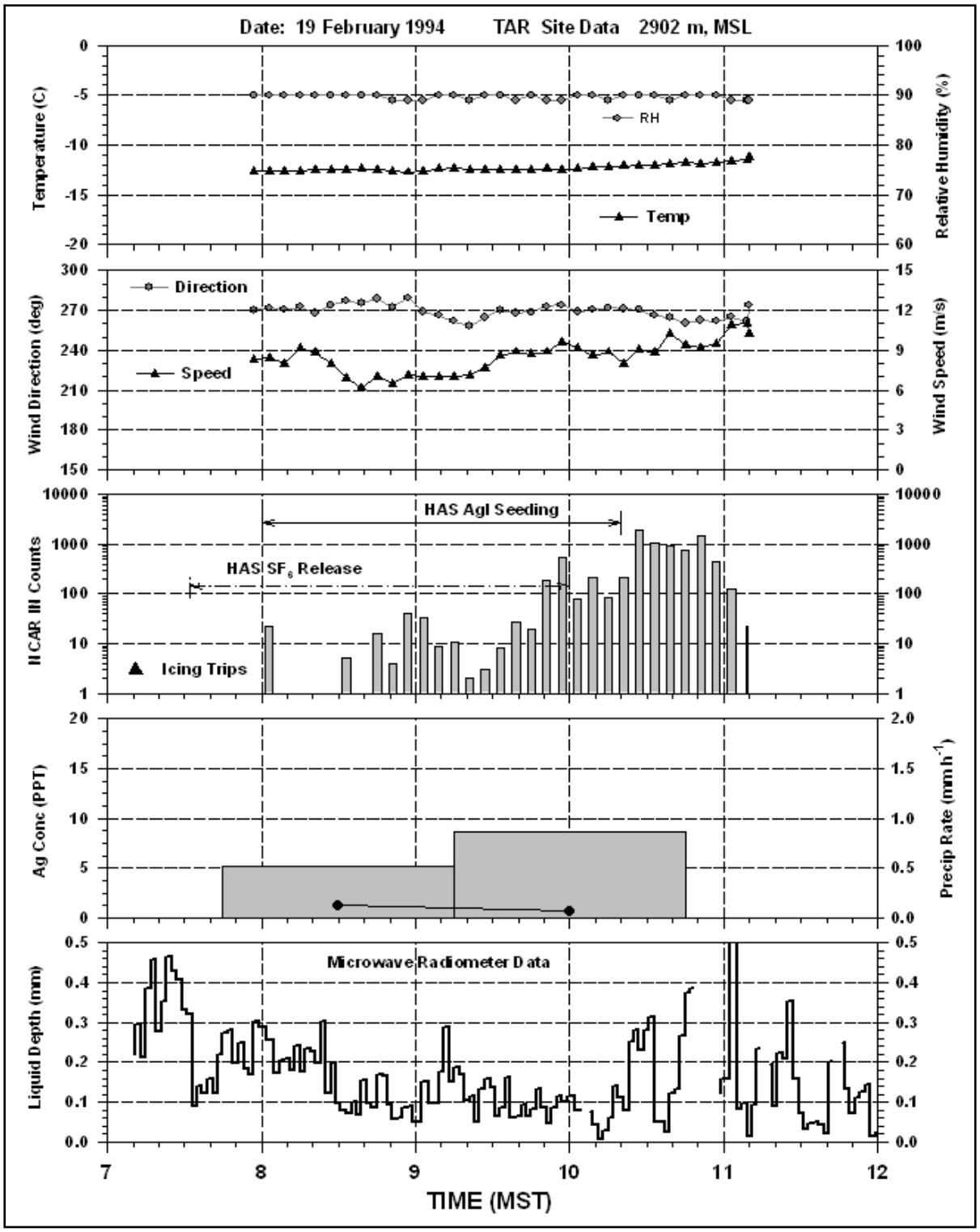

Figure 7. Meteorological data, ice nucleus counts, and snow chemistry observations observed at TAR from 0700 to 1200 MST (1400-1900 UTC) on 19 February 1994. Third panel also shows SF_6 and AgI release periods from HAS. Fourth panel shows the Ag concentration and precipitation rate from two snow samples collected at TAR. Bottom panel shows the RRS radiometer liquid water depth.

The meteorological criteria for conducting seeding experiments during the 1994 Utah field program were quite liberal but required cloud cover over the plateau with cloud base at or below the mountain top. Cross-barrier winds were required, as was the observation of SLW above the plateau from radiometer or mountain top icing detectors. For AgI seeding plateau top temperature needed to be < -5° C to ensure the chance of ice nucleation by AgI. Soundings, visual observations, plateau-top observations and aircraft observations verified that these conditions were met on 19 February. The shallow cloud depth of about one kilometer and the lack of any significant mesoscale forcing reduced the potential for natural precipitation, but the temperature regime in the cloud layer, the presence of SLW, and the weak westerly winds were quite conducive to seeding by AgI from the upwind side of the Wasatch Plateau. The weak winds allowed ample time for ice crystal growth and fallout over the ~10km width (~30 min transit time at 5.5 m s^{-1}) of the plateau top, provided seeding material nucleated significant numbers of ice crystals at or upwind of the western edge of the plateau. In fact the winds, the relative cold plateau-top temperature and the observation of continuous SLW indicated ideal AgI seeding conditions.

The experiment on 19 February began with the release of SF_6 from HAS at 0730. The MSU AgI generator was started at 0800. SF_6 and AgI were released only from the HAS high altitude site. The SF_6 release continued until 1015, although the release rate dropped off markedly after about 0955 (Fig. 5). The AgI generator was operated until 1020. At about the time seeding began project personnel began data collection with the NCAR counter and the K_a-band radar at RRS, and with the PMS 2D-C probe and NCAR counter at TAR. Snowfall collections also began at TAR. Operation of the instrumented mobile van began on the plateau-top highways, and the NOAA research aircraft took off from the Provo Airport at 0800 to initiate flight tracks over the plateau.

4. Results of the 19 February AgI Seeding Experiment

A. Characteristics of the Aerosol Plume

The instrumented van and research aircraft were very successful in detecting the AgI and SF_6 plumes during the experiment. The van found the plume along the upwind section of Highway 31, as well as on top of the Plateau between RRS and TAR. The aircraft detected the plume on both of the standard barrier-parallel east and west tracks, as well as on a north-south track about 9 km downwind of TAR. From research aircraft data the plume was detected at altitudes between 3150 and 3600 m (-15° to -18° C). As noted with several other 1994 cases, the plume was limited in vertical extent to about 700 m above the Plateau. Figure 8 summarizes the plume interceptions of both the van and aircraft, and provides a clear picture of its horizontal extent.

In Fig. 8 van detection of the SF_6 plume at concentrations greater than background (essentially 0 PPT) is shown with triangles and aircraft detection is shown with diamonds. The van detected the plume between 0839 and 1053, and the aircraft found evidence of the plume between 0823 and 1026. Specific times of detection are annotated on Fig. 8. (Note that the SF_6 plume locations are shown because of the faster response of this instrument compared to the NCAR counter, and the fact that that times in the data set were corrected for any time lag in response. The time required to purge the NCAR counter of IN after exiting the plume led to much greater uncertainty regarding the location of the trailing edge.) Figure 8 indicates that over its lifetime the aerosol plume passed over five of the plateau-top gages, while two gages were north of it and two well to the south. The data from RRS in Fig. 6 verify that the plume did not impact this site, and Fig. 7 shows that the plume's highest concentrations over the target site began about 1.5 hours after seeding began. Since the travel time to TAR was only about 40 min, this suggests the plume transport direction likely changed somewhat during the seeding period. The clockwise curve to the plume shape in Fig. 8 agrees well with the winds measured across the plateau which turned from about 230° at the release site to 250° at RRS, and further to 270° at TAR.

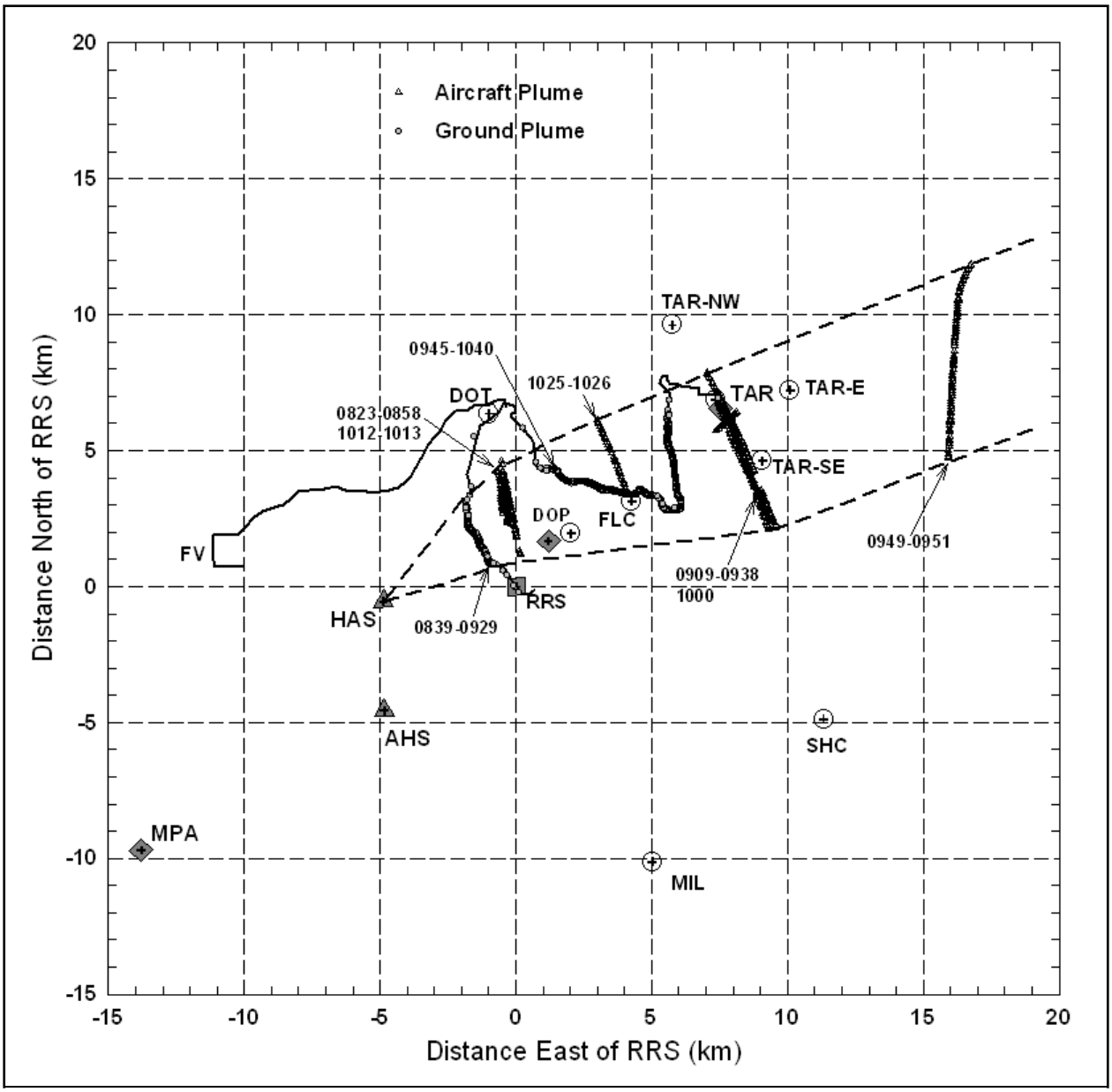

Figure 8. Horizontal grid showing instrument site locations and locations where the aerosol plume released from HAS was detected by the mobile van and the research aircraft on 19 February 1994. The main instrument sites are shown by gray-shaded triangles (seeding sites), diamonds and boxes. Precipitation gage locations are shown by circles.

The various van and aircraft plume dimensions and positions led to horizontal spread rate estimates of 1.1 - 2.6 m s^{-1} using a 5 m s^{-1} wind speed near the surface and a 6 m s^{-1}wind speed aloft. The plume horizontal and vertical spread rate estimates are summarized in Table 1. The average angular dimension of the plume was about 16°, quite similar to plume measurements made during other Utah experiments (Super, 1999) and other areas (*e.g.*, Holroyd and Super, 1988). In order for the aircraft to detect the plume on the west track, it would have needed to rise at a rate of at least 0.6 m s^{-1} from its release point at HAS.

Table 1. Aerosol plume characteristics from the 19 February ground seeding experiment. For plume spread rate estimates the average wind speeds shown in the second column were used. The vertical plume rise estimate was based solely on the aircraft data from the westernmost flight track.

Instrument Platform	Wind Speed (m/s)	Distance from HAS (km)	Time from HAS (min)	Plume Width (km)	Horizontal Spread Rate (m/s)	Vertical Spread Rate (m/s)
Van	5	4.0	13.3	0.9	1.1	-
Aircraft	6	5.8	16.1	2.3	2.4	0.7
Aircraft	6	10.0	27.8	3.5	2.1	-
Aircraft	6	14.3	39.7	6.3	2.6	-
Aircraft	6	22.9	63.6	7.2	1.9	-

B. Microphysical Characteristics of the Natural and Seeded Cloud Regions

Since the seeding plume did not impact RRS, and TAR was affected mostly by just the aerosol plume, the primary data set for determining microphysical responses to seeding came from the NOAA aircraft. The aircraft made 14 passes in the altitude range 3100-3800 m in the vicinity of the seeding plume shown in Fig. 8. The aerosol plume was detected on 12 of the passes, and a microphysical response to seeding was detected on 11 of the passes. One pass at 3700 m failed to detect cloud or aerosol, and in general cloud particles and the aerosol plume were found below 3600 m. Neither aerosol nor ice crystals were detected on the final pass of the day on the west track (16 min downwind) about 25 min after seeding ended, so it is very likely that the plumes were downwind of the west track by this time.

At the beginning of the seeding experiment a relatively large area of radar echo was moving south to north over the Wasatch Plateau. Seeding began just as this echo was passing to the north of the eventual plume location in Fig. 8, and subsequent observations will show that this was the most significant natural cloud feature to be sampled during the course of the experiment. Figure 9 shows the flight track and data from the first pass by the research aircraft through the seeding plume. The aerosol plume (bottom right panel) was encountered at 3400 m at a temperature of -16^{o} about 4 km northeast of HAS (shown on the flight track). The region of ice crystals encountered just north of the aerosol plume was within the radar echo that had moved just beyond the plume region. Concentrations ranged from 5 to 23 L^{-1}. A separate ice crystal concentration maximum of nearly the same magnitude was located within the aerosol plume boundary (3rd right panel). The precipitation rate estimates shown in the third panel of Fig. 9 were computed using the 2D-C analysis technique employed by Holroyd et al. (1995). The estimated rates ranged from 0.02 to 0.06 mm h^{-1}, and were similar inside and outside (north of) the seeding plume.

Liquid water content was less than 0.1 g m^{-3} in the natural cloud region north of the plume, and was nearly zero within the seeding plume. Two larger LWC maxima existed just south of the seeding plume. Not shown in Fig. 9 are the cloud droplet data from the aircraft FSSP. Throughout the flight droplet concentrations rarely exceeded 150 cm^{-3}, and were generally in the range of 50-100 cm^{-3}.

The 2D-C particle images revealed crystal types (habits) dominated by small thin plates (images with white centers) in the 100-150 μm diameter range in the region north of the seeding plume. In addition, larger particles at least 800 μm in diameter comprised of heavily rimed crystals, rimed sectored plates and aggregates were also sampled. Within the plume the predominant habits were rimed sectored plates and graupel in the 200-500 μm size range. There were very few aggregates and the concentration of particles >100 μm was similar to that in the north non-seeded region. In the region south of the aerosol plume, where particles >100 μm numbered less than 2 L^{-1}, the particles consisted of graupel and very small thin plates.

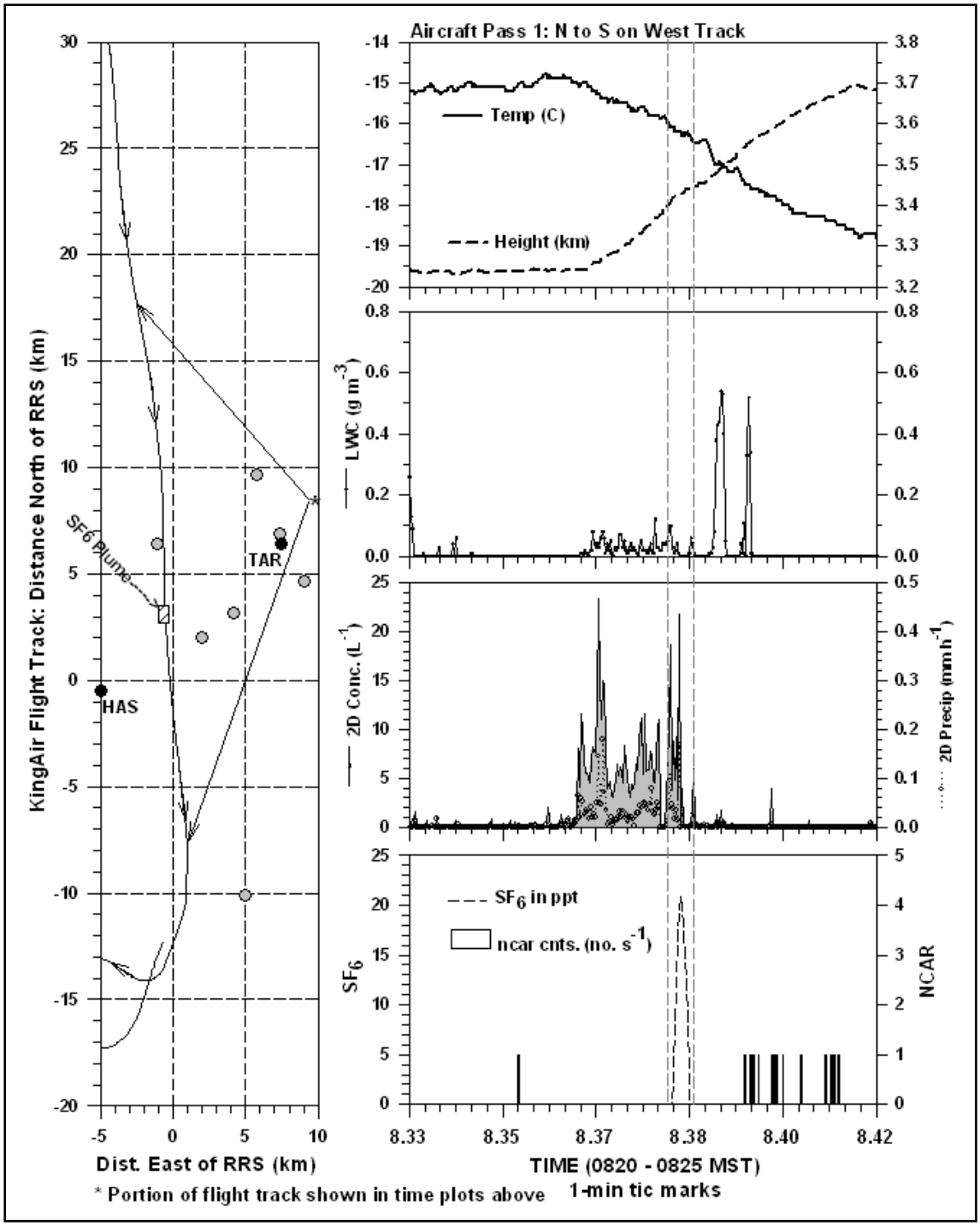

Figure 9. NOAA research aircraft flight track during first north to south pass through the seeding plume on 19 February 1994 (left panel). Seeding site (HAS) and target site (TAR) are shown as are precipitation gage sites (gray circles). The period of data shown in the panels on the right is identified by the two arrows from the point * on the left panel. Right panels show temperature and height (top), LWC (2nd), 2D-C ice crystal concentration and precipitation rate for particles >100 microns (3rd) and SF_6 and NCAR data (bottom).

On the second pass through the plume on the west track at an altitude about 200 m lower than Pass 1, the SF_6 plume was three times wider and the its concentration was 15 times greater. The ice particle concentrations north and south of the plume location were less than 1 L^{-1} compared to the peak in-plume concentration of 25 L^{-1}. The LWC south of the plume peaked at about 0.5 g m^{-1} in regions with almost no ice particles, while the average LWC in the plume was less than 0.1 g m^{-3}. Particles outside the plume were irregular in shape, some pristine and some rimed. In the plume particles were primarily rimed sectored plates in the 300-600 μm size range.

On the third pass on the west track at 3700 m neither the aerosol plume nor cloud particles were detected. The fourth pass at 3200-3300 m on the west track revealed an aerosol plume width of about 3 km with a peak SF_6 concentration similar to Pass 2. The in-plume ice particle concentration reached 30 L^{-1}, an enhancement of >30 times the concentration measured in the north and south non-seeded regions. In contrast, LWC was 0.3-0.4 on both north and south sides of the plume, while the plume LWC peaked at only 0.1 gm m^{-3}. Although a few large aggregates were found in the plume, the habits and sizes were similar to those on Pass 2 and were consistent with ice particles expected in the plate regime at -15° to -17° C.

The first four aircraft passes gave strong indications that seeding from HAS was enhancing the ice crystal concentrations in the shallow cloud over the plateau. Three of the passes also indicated that the liquid water in the plume was being depleted by the formation and growth of the ice particles. The ice particle sizes noted in the seeding plume at the aircraft altitudes were reasonable considering the transport time available between HAS and the west track. Crystals nucleated by AgI at or immediately downwind of HAS (substantiated by later radar observations) would have had 16 min or more to attain the size of the larger sectored plates (600-700 μm) noted at aircraft altitude. The variety of habits and sizes of particles indicated that the environment for crystal growth was not uniform, and this is verified by the sporadic nature of the observed cloud liquid. The peak liquid water contents of up to 0.5 g m^{-3} were indicative of embedded convection, and within these higher LWC regions the formation of moderate to heavily rimed particles is not surprising.

After the fourth pass across the seeding plume on the west track, the research aircraft made the next four passes on the east track (AC-2 in Fig. 2). The aerosol plume was identified on each pass at altitudes ranging from 3300 to 3600 m (-16° to -18° C). At the highest altitude on Pass 8 the aerosol plume was weaker and narrower, and the ice particle plume was also narrower with somewhat lower concentrations compared to the lower altitudes on Passes 5, 6, and 7. The plume interception point was 14.5 km downwind of HAS, equating to about a 43.6 min transit time.

The three passes at ~3400 m on the east track showed similar aerosol and ice particle characteristics. An example plot from Pass 7 between 0924 and 0933 is shown in Fig. 10. The LWC along the track was generally less than 0.2 gm m^{-3} and contents were similar within the plume compared to regions north and south of the plume. On all east track passes peak LWC was generally about half that observed on the west track. The aerosol plume consisted of two maxima, one quite broad with a peak concentration of ~200 PPT, and one narrower region with a peak of only about 20 PPT. The region of enhanced ice particle concentration was considerably broader than on the west track, and consisted of three distinct maxima. On all four east track passes the ice concentration within the aerosol plume had peaks of 25-30 L^{-1} while regions to the north and south of the plume had peak concentrations less than 5 L^{-1}, indicating an enhancement due to seeding by a factor of 5-6, or more.

The ice crystals within the seeding plume were predominantly rimed particles, often resembling graupel, and sizes varied considerably within the three peaks, but were nearly all less than 800 μm. A few sectored plates were present with varying amounts of rime. Examples of images within the seeding plume on Pass 7 are shown in Fig. 11. Images in the top panel of Fig. 11 were from the first concentration maximum inside the seeding plume and images in the bottom panel were from the third concentration maximum. The panels display particles at quite different stages of development where particles in the top panel could have formed at least 10 min prior, while the bottom panel shows very newly formed particles. This suggests that AgI continued to nucleate ice crystals across the plateau, possibly in new convective updrafts (indicated by the liquid water pattern on this and later passes). Images from the natural cloud region south of the seeding plume are shown in Fig. 12. The particles were a combination of very small plate-like particles and crystal aggregates several millimeters in size. Although the largest particles were much larger than those in the seeding plume, the estimated precipitation

was considerably lower due to the scarcity of these large particles. In Fig. 10 this region with relatively low concentrations of ice particles south of the plume represents a distance of about 20 km and was observed on radar as a broad region of echo that persisted during much of the experiment over the downwind edge of the plateau.

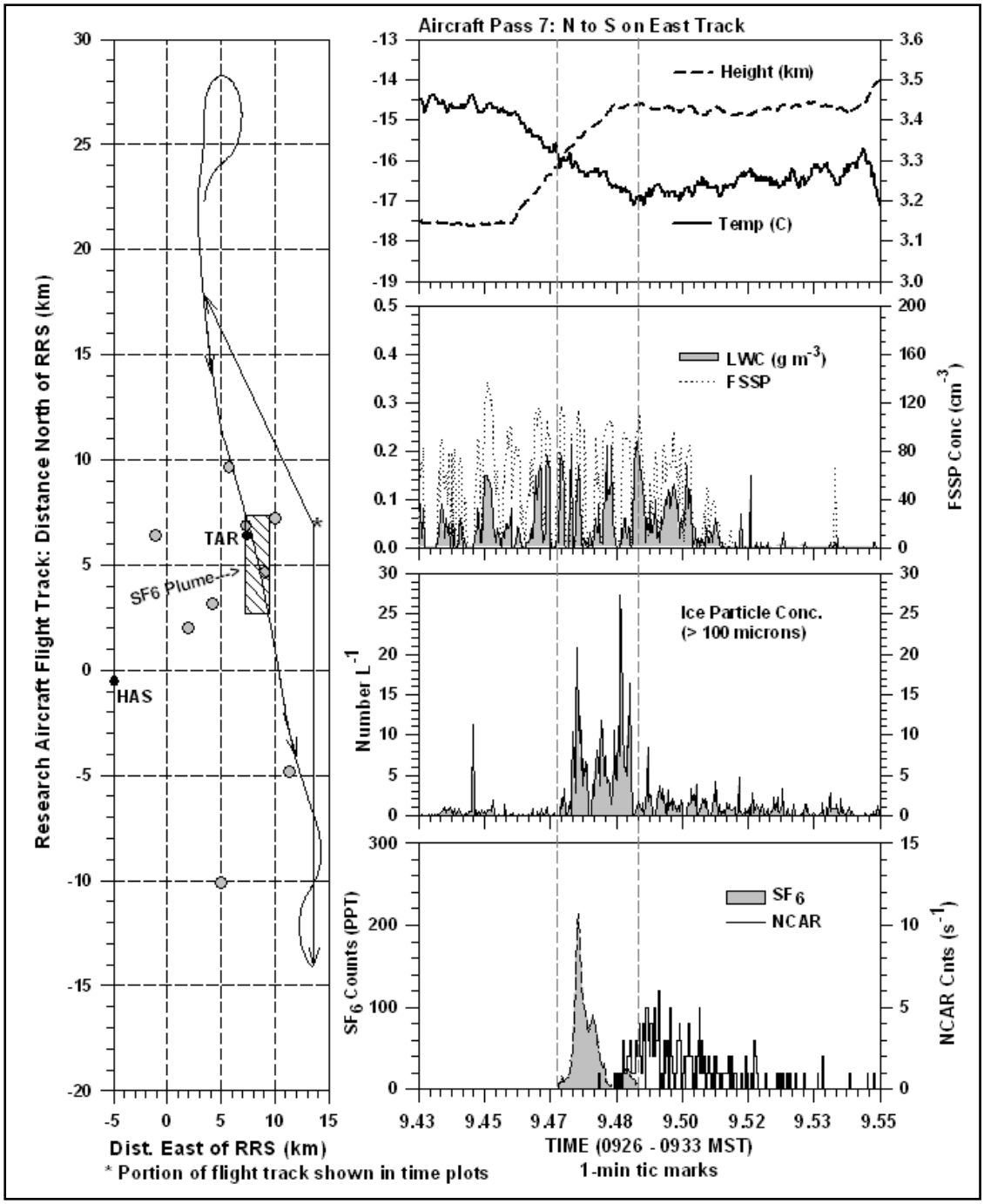

Figure 10. As in Fig. 9, except showing the flight track and data from the third pass (seventh overall) by the NOAA aircraft through the seeding plume on the east track. Second panel on the right shows both LWC and FSSP concentration, and third panel shows only ice particle concentration.

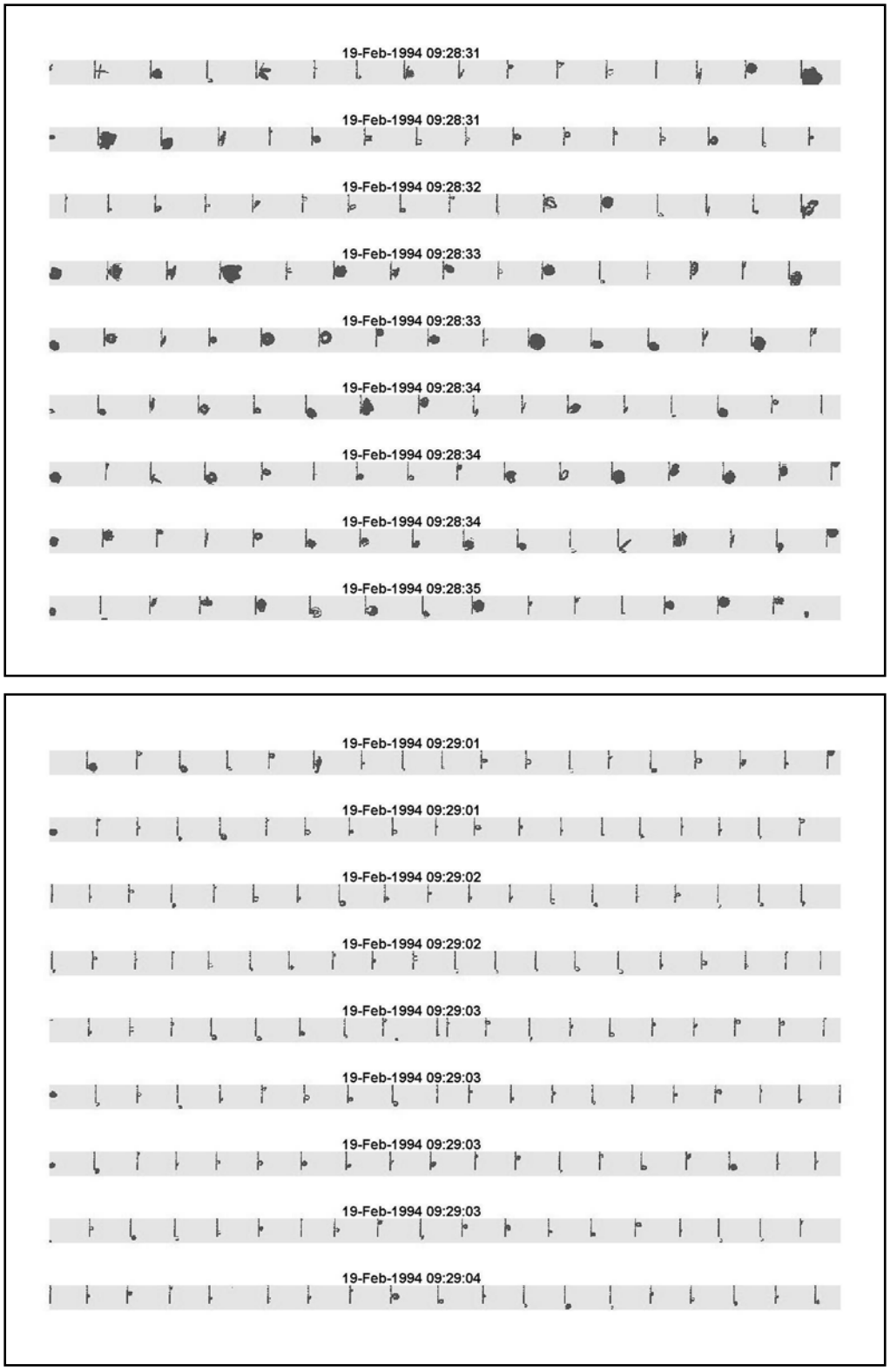

Figure 11. 2D-C particle images recorded within the seeding plume boundary (see Fig. 10) during Pass 7 on the east track. Top: Images from within the first concentration maximum in Fig. 10. Bottom: Images from within the third concentration maximum in Fig. 10.

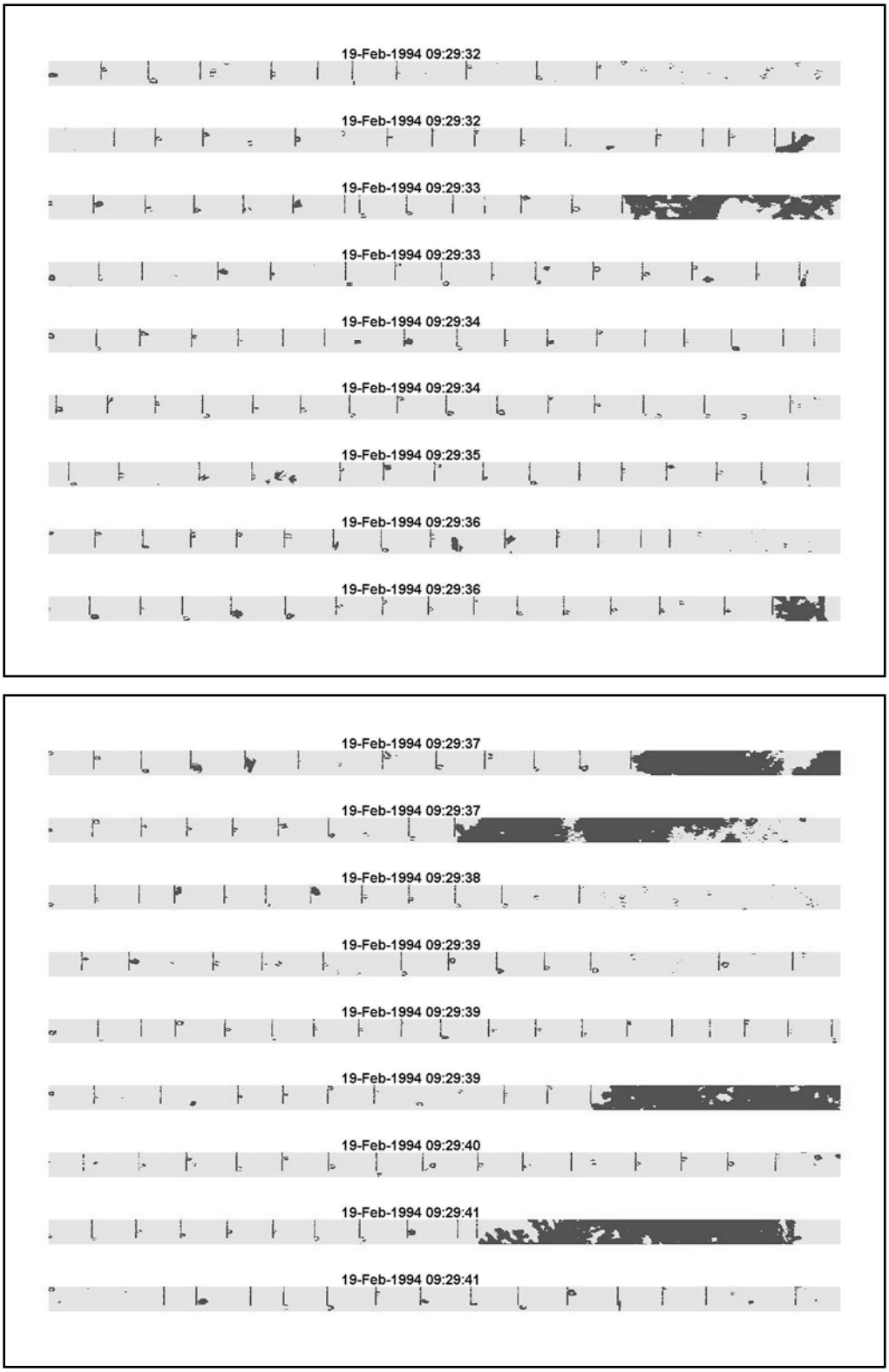

Figure 12. 2D-C particle images recorded just south of the seeding plume boundary (see Fig. 10) during the research aircraft Pass 7 on the east track.

Before the final passes on the west track were made one pass about eight kilometers downwind of the east track was made at 3500 m. Although this was over terrain that sloped downward to the east, LWC similar to that found on the east track was sampled 5-8 km south of the seeding plume in narrow peaks that again suggested convective cloud elements. The aerosol plume (IN and SF_6) was split into two distinct branches, each of which had, embedded within it, ice crystal concentrations ≤ 10 L^{-1}. The plume particles consisted mostly of small graupel (≤ 400 μm) with some thin plates.

Four final passes were made on the west track between 1010 and 1050. There seemed to be a resurgence of cloud liquid with three of the passes showing liquid water in discrete peaks along the flight path both south and north of the seeding plume. Several LWC maxima south of the seeding plume reached 0.4-0.5 g m^{-3}, likely reflecting the greater convective instability noted on the sounding at 1100. Passes 11, 12 and 13 revealed narrow aerosol and ice particle plumes quite similar to those found on the initial four passes on the west track. Ice particles in the seeding plumes were also again dominated by sectored plates up to 800 μm in diameter with varying degrees of rime, and graupel particles. The final pass on the west track (25-32 min after seeding ended) revealed no aerosol plume or ice crystal plume in the region where both had previously been detected. However, liquid water was plentiful (with little natural ice) along a 35 km region centered on the earlier plume location.

The aircraft ice particle observations from all passes where a seeding plume was detected are summarized in Table 2 and the averages of ice particle concentration, LWC and SF_6 concentration are plotted in Fig. 13 relative to the time and distance from HAS. The comparison of ice particle concentrations and computed precipitation rates for seeded and non-seeded cloud regions followed the method of Holroyd et al. (1995), hereafter referred to as HR95. A 1-km wide "buffer" region immediately adjacent to the seeding plume was ignored in the analysis. The non-seeded analysis regions were north and south of the buffer regions, and roughly equal in width (a minimum of 1-km wide) to the seeding plume. The seeded zone was defined by the period when SF_6 was detected, except for Pass 13 when it was estimated by the beginning time of NCAR counts minus 45 sec, with the period defined by the Pass 12 width of the SF_6 plume. For every pass with a plume detected the ice particle concentrations were greatly enhanced in the seeded zone, with the seed to no-seed ratio being generally greater than 10. The average par-

Table 2. Aircraft 2D-C ice particle concentrations (sizes > 100 μm) and estimates of precipitation rates from seeded and non-seeded cloud regions during the 19 February 1994 seeding experiment. Concentrations are averages (L^{-1}) across the seeding plume or no-seed regions. Precipitation estimates are in mm h^{-1}. Avg. N-S represents the average of the north and south no-seed regions. In column 7 "Seed" refers to the Plume 2D Conc. and "No-Seed" refers to the Avg. N-S Conc. Column 12 is similar except for using Plume 2D Precip. and Avg. N-S Precip.

Aircraft Pass	Track	North 2D Conc.	Plume 2D Conc	South 2D Conc	Avg. N-S Conc.	Ratio Seed/ No-Seed Conc.	North 2D Precip.	Plume 2D Precip.	South 2D Precip.	Avg. N-S Precip.	Ratio Seed/No-Seed Precip
1	W	5.940	4.800	0.790	3.365	1.43	0.0300	0.030	0.0040	0.017	1.76
2	W	0.039	4.993	2.585	1.312	3.81	0.0005	0.022	0.0125	0.0065	3.385
3	W	0.259	6.518	0.216	0.237	27.50	0.0011	0.066	0.0008	0.0009	73.33
5	E	0.102	7.941	1.245	0.673	11.80	0.0003	0.039	0.0032	0.0017	22.94
6	E	0.002	7.188	1.425	0.713	10.08	0.0000	0.033	0.0130	0.0065	5.08
7	E	0.216	5.790	1.416	0.816	7.10	0.0007	0.033	0.0041	0.0024	13.75
8	E	0.000	7.325	0.341	0.170	43.09	0.0000	0.033	0.0038	0.0019	17.37
9	Far E	0.075	1.630	0.176	0.125	13.04	0.0004	0.006	0.0017	0.0010	6.00
11	W	0.000	6.734	1.691	0.845	7.97	0.0000	0.032	0.0078	0.0039	8.20
12	W	0.045	5.279	0.000	0.022	239.95	0.0001	0.025	0.0000	0.0001	250.00
13	W	1.078	15.640	0.282	0.680	23.00	0.0055	0.061	0.0016	0.0035	17.43

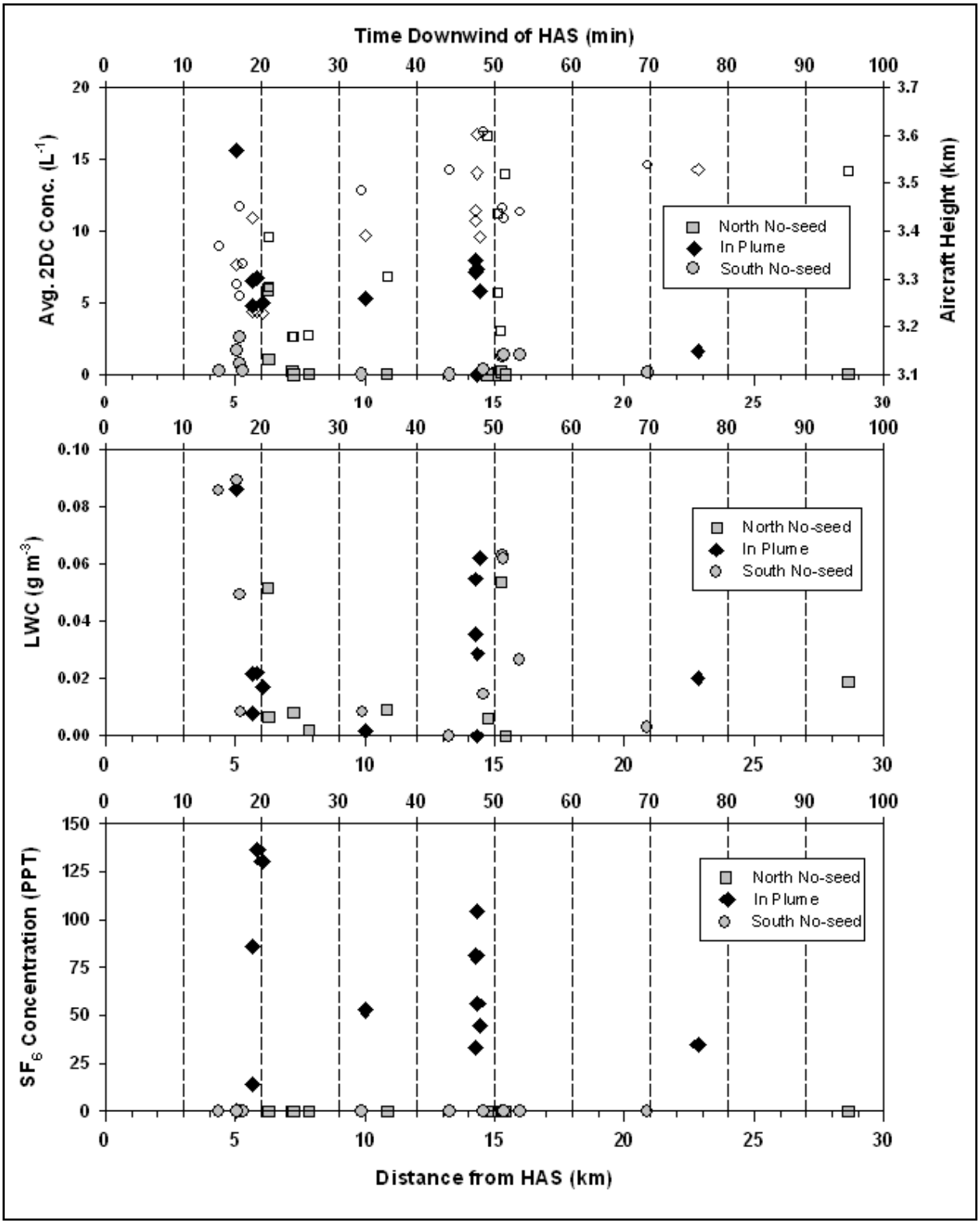

Figure 13. Average values of NOAA aircraft ice particle concentrations (top), liquid water contents (middle) and SF_6 concentrations plotted versus time and distance downwind of the HAS seeding site. Top panel also includes the aircraft altitude (open symbols) at each data point.

ticle concentrations in the seeded zones on the west track ranged from 4.8 to 15.6 L^{-1}, somewhat smaller than values reported by HR95 who found concentrations up to 54.1 L^{-1}. In the current study concentrations in the east track seeded zone were very consistent, ranging from 5.8 to 7.9 L^{-1} on four passes and these were generally larger than those found by HR95.

Table 2 indicates that the estimated precipitation rates from the aircraft 2D data were quite small, all being less than 0.1 mm h^{-1}. However, these rates, with a few exceptions, are comparable to those found by HR95. The ground-based 2D data from HR95 (missing in this case) revealed estimated rates at the surface that were 2-10 time greater than at aircraft altitude. This indicated that considerable particle growth occurred in the ~300 m of cloud between the surface and the aircraft. With the liquid water contents observed in the current case study, significant particle growth by cloud water accretion would also been expected on 19 February.

There were numerous and significant differences in the microphysical observations of this 19 February case and the 21 February case described in HR95. These were likely due to the environmental conditions which were notably different on the two days. In particular the HR95 case took place under more stable conditions, had much less cloud water available (generally 0.05 g m^{-3} or less at aircraft altitude), had warmer temperatures in the layer between the seeding generator and the top of the plateau (-6° to -9° C), and showed a significant decrease in cloud liquid across the plateau. HR95 found that precipitation from seeding was most likely due to rapid nucleation of ice near the generator site, followed by growth and formation of aggregates to 1 mm size which subsequently fell to the surface near the upwind edge of the plateau. Ice crystal and precipitation enhancement in the seeding plume were not nearly as evident from the center to the downwind side of the plateau. These differences will be discussed further after the presentation of the radar and precipitation results from the current study.

C. Evidence of Seeding Effects in the Ka-band Radar Data

Although the results of analyses of the aerosol plume and the aircraft microphysical data suggest a continuous plume of seeding effect across the plateau, the measurements were from discrete locations and do not truly describe the areal extent of seeding effects. One unique aspect of the 19 February case was the apparent seeding effect noted in the K_a-band radar data in real time. Prior to the start of seeding radar echoes covered areas upwind and downwind of the RRS site (Figs. 1 and 2). At least one small precipitation band moved across the area from southwest to northeast. Following the passage of the band, echoes upwind of RRS began to diminish, and only weak scattered returns remained over the top of the Plateau.

At the start of seeding near 0800 the natural echo band noted previously was about 5 km north of RRS. There was no obvious structure to the echo pattern downwind of RRS. By 0823, 20 min after the start of seeding, there was some enhanced echo over the west portion of the plateau, but the echo had not taken on a distinct plume shape. There was also a region of weak echo, oriented north-south, over the downwind edge of the plateau, and this feature was observed throughout the seeding experiment. The plume-like echo structure extending downwind of HAS and across most of the plateau became obvious at about 0851, or 51 min after the start of seeding. With the 5-6 m s^{-1} winds documented over the plateau the leading edge of the seeding plume could have been 15-16 km downwind and ice crystals nucleated near the generator site could easily have been radar detectable along the length of the plume.

The elongated radar echo at 0851 was oriented east-west and fell entirely within the outline of the aerosol plume shown in Fig. 8. The radar echo plume structure was most obvious between 0900 and about 1020, after which time it began to dissipate. Figure 14 shows three sector scans taken at 0908, 0930 and 1007. The line segment across the radar echo at each time represents the aerosol plume location detected by the aircraft at a similar time. At 0908 the aircraft was on the east track and found an ice crystal plume at the echo plume location similar to that in Fig. 9 with particles being mainly small rimed crystals and grau-

pel. The enhanced echo plume was over both the TAR-SE and FLC gages shown in Fig. 8. To the south of the seeding plume the aircraft passed through the small enhanced echo region seen on the 0908 radar image and encountered low concentrations of large aggregates and very small thin plates.

The 0930 image in Fig. 14 shows the echo plume corresponding to the aerosol seeding plume to be relatively uniform and continuous across the plateau, and extending well downwind of the eastern edge. The aircraft pass on the east track was at nearly the same time, with the aerosol plume encountered from 0928 to 0929:30 at the location indicated in Fig. 14. The radar beam center was also very close to the aircraft altitude at this location, so the ice particles encountered by the aircraft were those contributing to the radar echo plume. At the surface the TAR-SE and FLC gages were still beneath the enhanced radar plume. Although this sector scan did not extend as far to the south, the natural echo region apparently still persisted since the aircraft again encountered low concentrations of large aggregates to the south of the seeding plume.

With time the echo plume shifted gradually northward so that the northern edge was close to the TAR site, and the enhanced portion was also eventually over the TAR-E gage (Fig. 8). Although there were several times when the upwind edge of the echo plume could be identified, the last sector scan in Fig. 14 taken at 1007 was one of the best to show the origin of the echo plume just slightly more than one kilometer to the northeast of the HAS seeding site. The radar beam height at the tip of the echo plume was 3027 m, 534 m above hAS. Using a 4 m s-1 wind speed for the average in the layer between the seeding generator and the echo height, the echo edge would have been about 4.2 min downwind of HAS. For radar detection at this location, a seeding plume ascent rate of about 2 m s-1 would have been required, in addition to ice nucleation quite close to the generator in order for crystals to grow large enough to become radar detectable.

Shortly after 1007 the aircraft detected the seeding plume at the location shown in Fig. 14 and found ice particles (mainly rimed sectored plates) in concentrations of 10-30 L^{-1} and sizes to 700 μm. The radar echo plume was not nearly as uniform as at 0930, and the enhanced region of 40+ dBm was over the western side of the plateau. The FLC gage continued to be beneath the echo plume. Note again the persistent enhanced echo south of the plume near the downwind edge of the plateau. The radar observer frequently noted this echo downwind of RRS and indicated that it appeared to develop over and downwind of minor ridges to the east of RRS, and stayed somewhat tied to these terrain features. The echo plume remained detectable through about 1020, after which time there was still an enhanced region, but it was mainly in the region 6-12 km east of RRS. At 1039, 22 min after seeding ended, the upwind portion of the plume had dissipated, but further downwind the FLC gage was still under enhanced echo as was the TAR-SE gage.

The radar data were analyzed in small 2x2 km boxes centered on each gage site to determine the time history of reflectivity over each gage. The data were taken from all sector scans, PPIs and RHIs recorded on 19 February. A uniform grid of reflectivity values was then created with a time interval of 5 min and a height interval of 50 m using a distance-weighting interpolation on the actual data points. The dBm values shown in Fig. 14 were first converted to values of dBZ_i using the refractive index for ice and the measured, or computed, radar parameters. A contoured plot of the interpolated values for FLC is shown in Fig. 15. A region of enhanced reflectivity is indicated from about 0840 to 1130 in close agreement with the time period when the seeding plume was expected to be over FLC. The small scale reflectivity maxima visible in this period are likely due to the convective nature of the clouds which was noted in the aircraft liquid water and ice particle characteristics (and also by the aircraft scientist). The reflectivity pattern over FLC differed markedly from that over a gage to the north of the seeding plume (TAR-NW) which is shown in Fig. 16. Here the echo strength is generally less than -7 dBZ_i, with no significant echo enhancement noted during the seeding period.

Overall the radar results are highly indicative of a seeding effect being produced by the AgI seeding on this day. The radar echo plume always fell within the boundary of the aerosol seeding plume identified by ground and aircraft sensors. The enhanced echo plume also matched locations where the aircraft detected enhancement in ice crystal concentration. The detection of the echo

plume a very short distance (time) from the seeding site also suggested that ice nucleation occurred very rapidly, likely by the forced condensation-freezing mechanism described by Finnegan and Pitter (1988). Contact nucleation and ice particle growth would have required a much longer time period, particularly with the relatively low cloud droplet concentrations noted on this day. The relatively uniform pattern at times noted in the radar echo plume also suggested ice particles were being produced throughout the cloud volume affected by the seeding plume, but that enhanced precipitation was more likely to have come from "pockets" of convection where ice particle growth was enhanced greatly by the riming process. This hypothesis is reinforced by the aircraft observation of mainly highly rimed particles within the seeding plume, but accompanied by small thin unrimed plates generally at the edges of the plume.

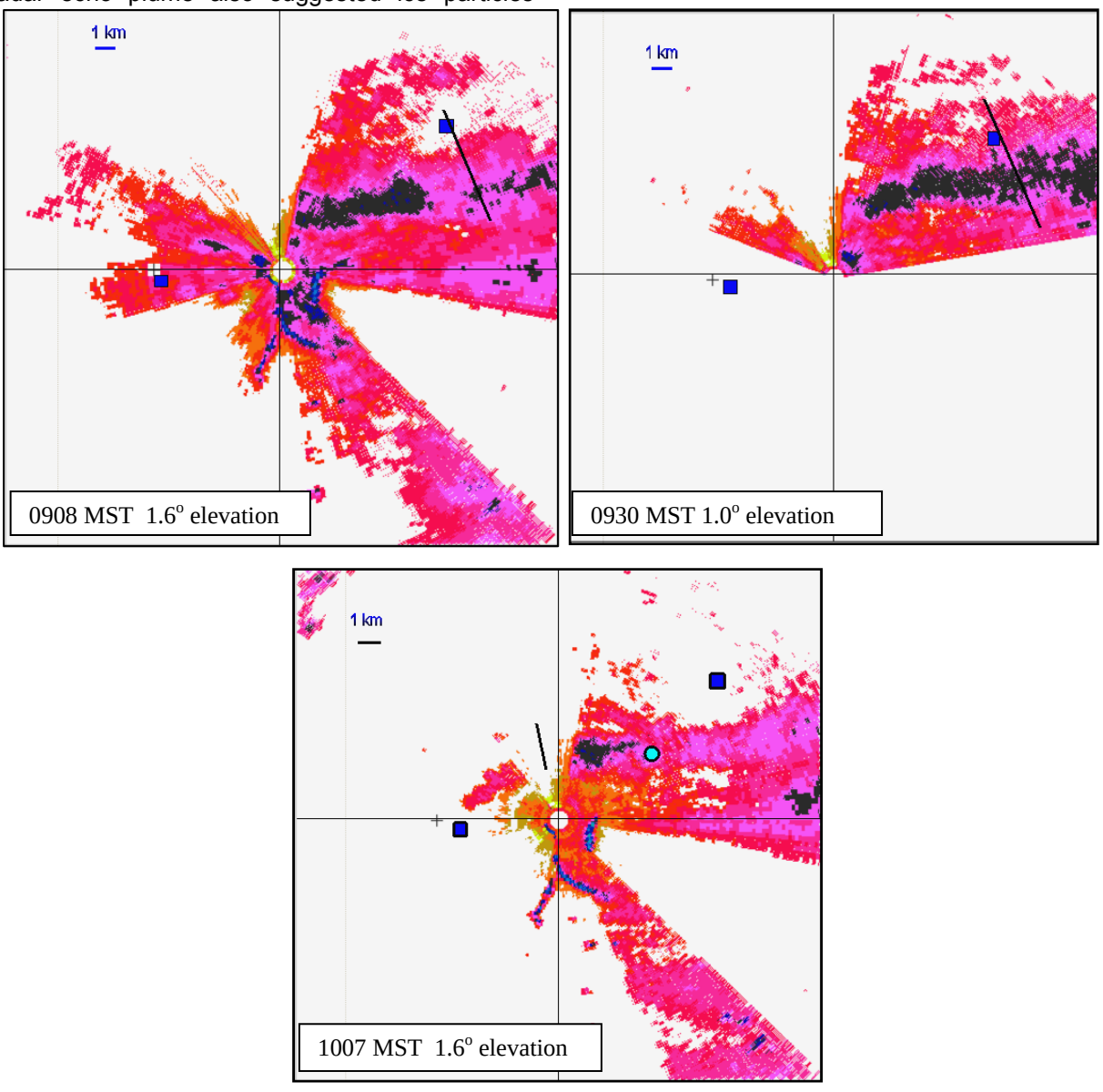

Figure 14. PPI images from the K_a-band radar at RRS. Color shading is in 10 dBm intervals with the outer pink being 20 dBm and the inner dark gray being 40 dBm. The notch to the northeast of the radar is due to blockage by trees and the narrow blue shaded echoes southeast through south-southwest of the radar are ground clutter. RRS is at the center of each image. The blue square to the west is the HAS seeding site and the blue square to the northeast is the target site (TAR). Black line segments in each image show regions where the research aircraft detected the seeding plume.

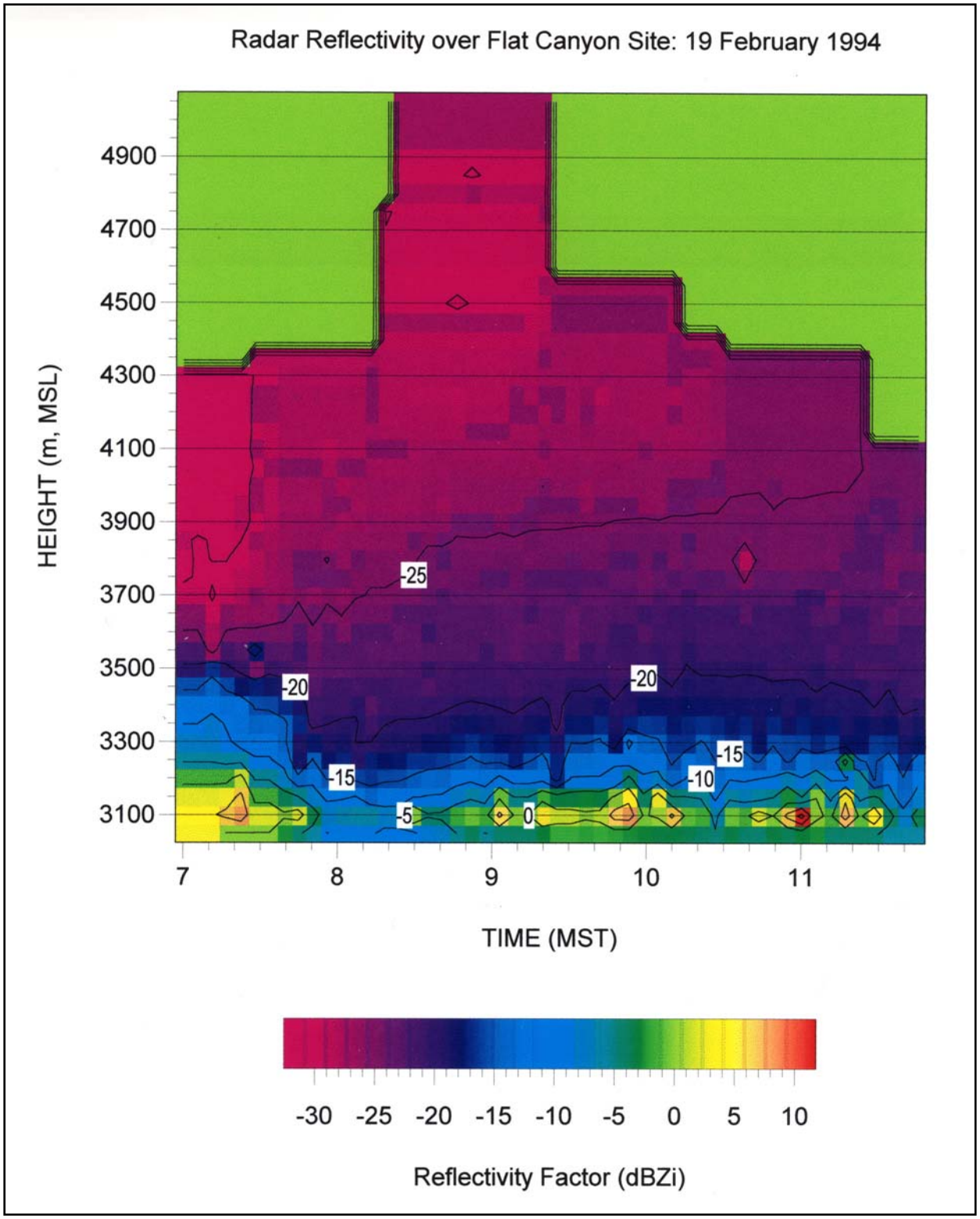

Figure 15. Time versus height profile of reflectivity factor relative to ice scatterers (dBZ_i) constructed from range bins over the FLC gage location (see Fig. 8) using data from the RRS K_a-band radar PPIs, sector scans and RHIs on 19 February 1994.

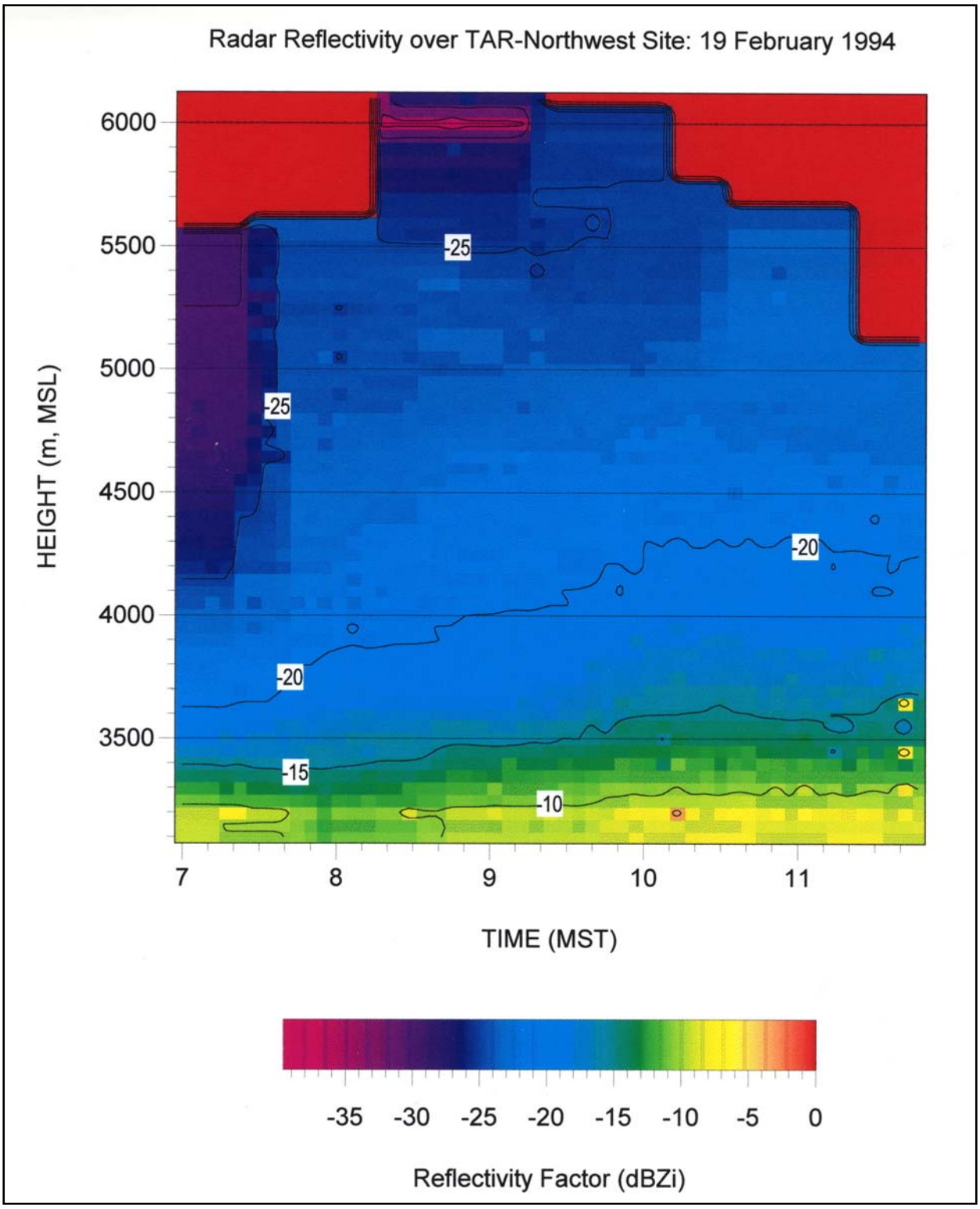

Figure 16. As in Fig. 15, except using radar data collected over the TAR-NW gage location shown in Fig. 8.

D. Evidence of Seeding Effects in the Precipitation Data

The quality of the precipitation data on this day was not particularly good. Several of the gages both inside and outside the seeding plume malfunctioned and the entire day's data from these gages were lost. The gages with no useable data were TAR-NW, DOP and MIL in Fig. 8. In addition, FLC and TAR had only partially useable records. The remaining good data from five gages north, within and south of the seeding plume are shown in Fig. 17. The estimated period of seeding effect at each gage is shown by the vertical dashed lines on each panel. The start time for the period of effect were obtained by moving an imaginary line oriented orthogonal to the seeding plume orientation (from ~250^{o}) across the plateau, beginning at the start of seeding, at the observed wind speed (~ 5 m s^{-1}) and noting the time at which this line crossed each gage. The end time was found the same way by moving the line beginning at the time that seeding ended.

The two gages (FLC and TAR-SE) that were most often found within the aerosol plume boundary and the radar echo plume showed a significant enhancement in precipitation during the period of effect compared to the gage to the north (DOT) and the gage to the south (SHC). The TAR ice nuclei data shown in Fig. 7, and the aircraft ice crystal and radar plume locations suggest that TAR precipitation could have been affected by seeding after about 1000. There is an indication of this in the slightly enhanced Ag content in the last snow sample taken at TAR, but the sample was very small and was collected over a period of nearly 1.5 hours, so the seeding signal is very weak at best.

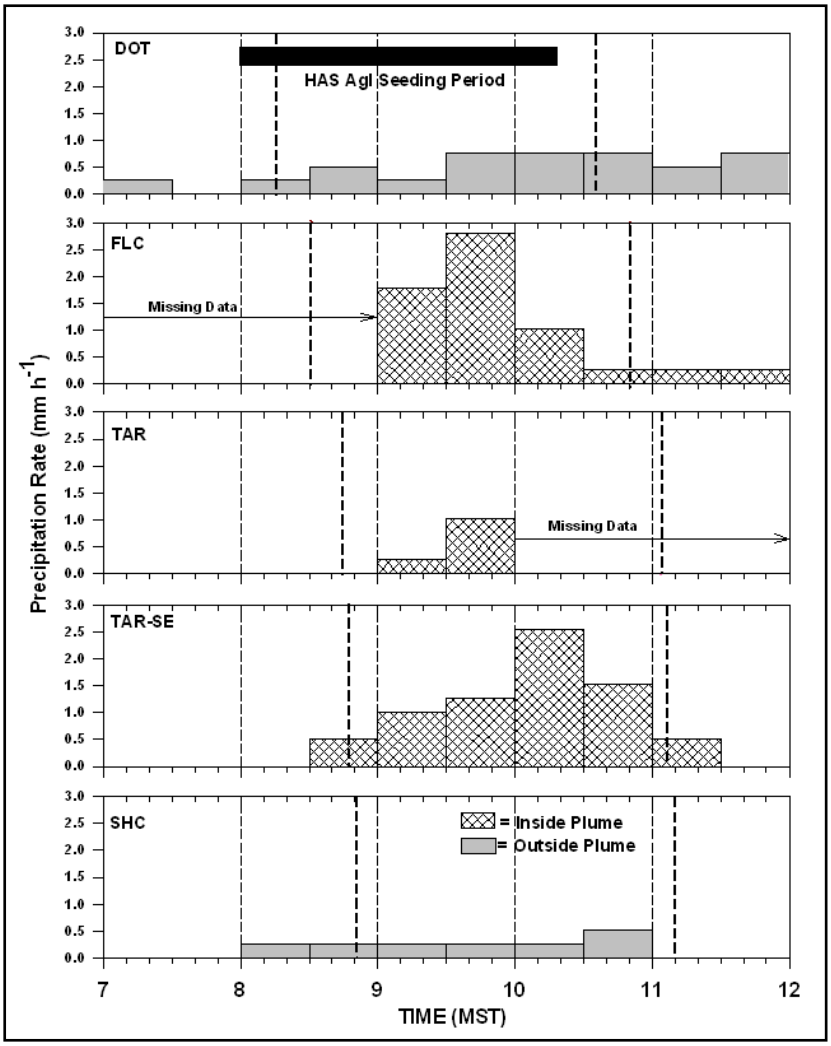

Figure 17. Precipitation recorded at five of the Wasatch Plateau gages on 19 February 1994. Top panel shows the period of AgI seeding at HAS. Dashed lines on each plot show the time period when each gage would have been affected by a plume from a site the same distance upwind as HAS. Shading indicates the gages that were within the actual seeding plume and ones that were outside the actual plume. See Fig. 8 for gage locations.

The precipitation rates noted at FLC and TAR-SE were much greater than those predicted by the 2D probe estimates at aircraft altitude, but a significant increase in particle size and mass would be expected in the 300-500 m of cloud between the aircraft and the ground. The measured rates were in reasonable agreement with the rates estimated by a K_a-band Z-S relationship (Matrosov, 1992) using the maximum reflectivity measured in the radar plume. The enhanced precipitation noted by FLC and TAR-SE in Fig. 17 corresponded quite well to the occurrence of the radar plume over these same gages. The average precipitation rate measured at FLC and TAR-SE within the seeding plume period was 1.52 mm h^{-1}, more than three times the average of two gages to the north (DOT) and south (SHC) of the plume (0.44 mm h^{-1}).

5. Summary of Results and Comparison with Other Seeding Experiments

The 19 February 1994 AgI seeding experiment verified all the points in the snowfall enhancement conceptual model presented by Super and Heimbach (1983). Seeding material was reliably produced and the transport of seeding material to a region of cloud with supercooled liquid water that was -10^{o} C or colder was verified. This temperature was low enough for significant ice crystal formation with the AgI nuclei used on the Utah project. This cloud temperature was also associated with the best positive seeding results from the Bridger Range Experiment. A significant enhancement of ice crystals above the natural background was verified in the seeded cloud zone. Crystal concentrations up to 50 L^{-1} were measured at aircraft altitudes and, though they were unavailable, ice concentrations at the surface would very likely have been much larger. Natural ice concentrations outside the seeding plume were generally less than 5 L^{-1}.

The wind direction carried the seeding material toward the target and wind speeds were relatively slow and allowed ample time for ice particle growth and fallout over the target area. Aircraft and surface data verified the aerosol plume dimension which spread downwind at an angle of about 16^{o}, in good agreement with earlier experiments on the Wasatch Plateau (Super, 1999), the Grand Mesa of Colorado (Holroyd et al., 1988) and the Bridger Range in Montana (Super, 1974). The plume characteristics were very similar to those described by HR95 during a similar type of experiment. The plume rise rate based on aircraft measurements about 6 km downwind of the seeding site was estimated as 0.6 m s^{-1}, but radar measurements within one kilometer of the seeding site indicated the ascent rate closer to the generator was approximately 2 m s^{-1}.

The microphysical response to seeding differed markedly from that described by Holroyd et al. (1995) for an experiment that occurred on 21 February, two days following the one presented here. The HR95 case, conducted in much lower liquid water conditions and somewhat warmer temperatures, indicated that seeding produced a high concentration of ice crystals close the seeding site that grew primarily by vapor deposition followed by aggregation. The relatively large aggregates fell out within about 5 km of the seeding site near the upwind edge of the plateau. Little response to seeding was noted beyond the center of the plateau and liquid water was almost entirely depleted. In the current case relatively large single crystals (sectored plates) grew by vapor deposition, but growth by accretion of cloud droplets appeared to be the dominant process within the seeding plumes. Rimed particles and graupel were noted in the plume across the width of the plateau, and although liquid water was less on the downwind side, liquid water contents of 0.2 g m^{-2} were still common near the downwind edge.

The response to seeding noted in the radar data was the most unique aspect of the current case. This was not observed in any of the several other successful seeding experiments conducted over the Wasatch Plateau in 1994. The lack of natural echo over the plateau for this case was likely the main reason for this success, but the extension of the microphysical seeding effect across the width of the plateau would also increased the likelihood of detection of the ice crystal plume by radar. The detection of the upwind edge of a radar echo plume (within the aerosol seeding plume) at a distance of only one kilometer from the seeding site strongly suggested that a rapid nucleation process occurred for this case, an observation in common with HR95. The convective nature of the orographic cloud on 19 February complicated attempts to estimate ice particle growth rates. Measurements on the west track at ~20 min downwind revealed sectored plates up to at least 700 μm in diameter. Assuming the crystals

were nucleated nearly instantly, this corresponds to a growth rate of 0.53 μm s^{-1} which is quite feasible for this crystal type and is also comparable to average rates documented by Deshler et al (1990) for aircraft seeding in the Sierra Nevada. However, the range of sizes observed on the west track indicates either a range of nucleation times or growth rates, or both. Also the larger particles could have fallen below the aircraft altitude. Growth rates could certainly have varied depending on whether crystals were inside or outside the higher liquid water zones.

The radar echo plume associated with the seeding plume indicated that the effect of the seeding extended across the plateau. The plume varied in intensity and width, but could be identified for about 1.5 hours starting about 50 min after the start of seeding. The highest reflectivity, and therefore the highest precipitation rate, was indicated to be in the range of 6-13 km downwind of the seeding generator. The FLC precipitation gage fell within this distance interval, and was the gage most frequently noted beneath the radar plume. Although the precipitation enhancement was based on a very small sample of observations, the indicated enhancement is not unlike results of individual seeding experiments in the Bridger Range where particle probe estimates of precipitation indicated a doubling of rates within seeded zones (Super and Heimbach, 1988). Super and Boe (1988) also showed a tripling of precipitation rates in seeded zones during Grand Mesa ground seeding experiments. The magnitude of the suggested seeding effect on precipitation (about 1.1 mm h^{-1}) was also documented in other Utah experiments (Super and Holroyd, 1997).

6. Discussion and Conclusions

This case study adds to the evidence of positive seeding effects from snowfall enhancement experiments that have been conducted under the guidelines of the conceptual model described by Super and Heimbach (1983). There have been some obvious case to case differences, but in large part the results of this case match the physical evidence previously reported from the Bridger Range, the Grand Mesa and the Wasatch Plateau. Two statistical experiments with positive and statistically significant results were either done in tandem with the physical experiments (Super and Heimbach, 1983), or evolved as a result of the physical experiments (Super and Heimbach, 2005). However, with only a limited number of past randomized experiments conducted under a similar design, it would be of great benefit to conduct such experiments on a scale considerably expanded beyond the original one to two seeding generator experiments. Such an experiment might be built around an existing operational program, as part of the research recommended by the 2003 NAS report.

This case showed the benefit of finding an additional tool with which to study the physical effects of cloud seeding. Some newer technologies such as short wavelength polarized radar have been designed since this program of the mid-1990s. The trace chemical techniques used to analyze cloud seeding effectiveness (*e. g.*, Warburton et al., 1995) can now be applied over basin-sized project areas and would add greatly to the evaluation of new experiments. These and other newer technologies, and advanced modeling capabilities, need to be included in the physical studies that should accompany any new randomized experiment.

Acknowledgements. Although this research was conducted more than a decade ago, the NOAA AMP is acknowledged for its funding support. The Utah/NOAA field program was supported by numerous people from the Utah Division of Water Resources, the U. S. Bureau of Reclamation, NOAA, the University of North Carolina at Asheville, and the Desert Research Institute. The author gratefully acknowledges the contributions of these organizations. In particular Mr. Clark Ogden, then with the State of Utah, is thanked for his logistical organization and great attitude. Special thanks go to Dr. Arlin Super for his leadership in all the scientific aspects of the program and to Dr. James Heimbach for producing very high quality data sets as the lead scientist on the NOAA King Air. Dr. Edmond Holroyd is thanked for locating and contributing the data from the aircraft 2DC probe, and Dr. Melanie Wetzel of DRI is thanked for recognizing the radar seeding effect in real time and carefully describing it in her operations notes.

6. References

DeMott, P. J., W. G. Finnegan and L. O. Grant, 1983: An application of chemical kinetic theory and methodology to characterize the ice nucleating properties of aerosols used for weather modification. *J. Climate Appl. Meteor.*, **22**, 1190-1203.

Deshler, T., D. W. Reynolds and A. W. Huggins, 1990: Physical response of winter orographic clouds over the Sierra Nevada to airborne seeding using dry ice or silver iodide. *J. Appl. Meteor.*, **29**, 288-330.

ERS, 2003: RAOB The complete RAwindsonde OBservation program (Version 5.7): User guide and technical manual. Environmental Research Services, Matamoras, PA, 88 pp.

Finnegan, W. G. and R. L. Pitter, 1988: Rapid ice nucleation by acetone-silver iodide generator aerosols. *J. Weather Mod.*, **20**, 51-53.

Heggli, M. F. and R. M. Rauber, 1988: Characteristics and evolution of supercooled liquid water in wintertime storms over the Sierra Nevada. *J. Appl. Meteor.*, **27**, 989-1015.

Holroyd, E. W., J. T. MacPartland and A. B. Super, 1988: Observations of silver iodide plumes of the Grand Mesa of Colorado. *J. Appl. Meteor.*, **27**, 1125-1144.

Holroyd, E. W., J. A. Heimbach and A. B. Super, 1995: Observations and model simulation of AgI seeding within a winter storm over Utah's Wasatch Plateau. *J. Weather Mod.*, **27**, 35-56.

Huggins, A. W., 1995: Mobile microwave radiometer observations: Spatial characteristics of supercooled cloud water and cloud seeding implications. *J. Appl. Meteor.*, **34**, 432-446.

Huggins, A. W., 1996: Use of radiometry in orographic cloud studies and the evaluation of ground-based cloud seeding plumes. 13th Conf. on Planned and Inadvertent Weather Modification, Amer. Meteor. Soc., Atlanta, Georgia, 142-149.

Matrosov, S. Y., 1992: Radar reflectivity in snowfall. *IEEE Transactions on Geoscience and Remote Sensing*, **30**, 454-461.

National Research Council (NRC), 2003: Critical issues in weather modification research, *The National Academies Press*, Washington, D. C., 131 pp.

Rauber, R. M. and L. O. Grant, 1986: The characteristics and distribution of cloud water over the mountains of northern Colorado during wintertime storms. Part II: Spatial variations and microphysical characteristics. *J. Climate and Appl. Meteor.*, **25**, 489-504.

Super, A. B., 1974: Silver iodide plume characteristics over the Bridger Mountain Range, Montana. *J. Appl. Meteor.*, **13**, 62-70.

Super, A. B. and J. A. Heimbach, 1983: Evaluation of the Bridger Range winter cloud seeding experiment using control gages. *J. Climate Appl. Meteor.*, 1989-2011.

Super, A. B. and J. A. Heimbach, 1988: Microphysical effects of wintertime cloud seeding with silver iodide over the Rocky Mountains. Part II: Observations over the Bridger Range, Montana. *J. Appl. Meteor.*, **27**, 1152-1165.

Super, A. B. and B. A. Boe, 1988: Microphysical effects of wintertime cloud seeding with silver iodide over the Rocky Mountains. Part III: Observations over the Grand Mesa, Colorado. *J. Appl. Meteor.*, **27**, 1166-1182.

Super, A. B. and E. W. Holroyd, 1997: Some physical evidence of AgI and liquid propane seeding effects on Utah's Wasatch Plateau. *J. Weather Mod.*, **29**, 8-32.

Super, A. B., 1999: Summary of the NOAA/Utah Atmospheric Modification Program: 1990-1998. *J. Weather Mod.*, **31**, 51-75.

Super, A. B. and J. A. Heimbach, 2005: Randomized propane seeding experiment: Wasatch Plateau, Utah. *J. Weather Mod.*, **37**, 35-66.

Warburton, J. A., S. K. Chai, R. H. Stone and L. G. Young, 1996: The assessment of snowpack enhancement by silver iodide cloud-seeding using the physics and chemistry of the snowfall. *J. Weather Mod.*, **28**, 19-28.